

# Progress and Challenges in $\text{LiMOCl}_4$ and $\text{NaMOCl}_4$ ( $M = \text{Nb, Ta}$ ) Oxyhalide Solid Electrolytes for Solid-State Batteries

Jon A. Newnham,\* Alexander G. Squires, Marvin A. Kraft, David O. Scanlon, and Wolfgang G. Zeier\*

The discovery of the  $\text{LiMOCl}_4$  ( $M = \text{Nb, Ta}$ ) oxyhalides is exciting for the field of solid-state batteries as they offer similar benefits to other halide solid electrolytes in terms of electrochemical stability, but with high ionic conductivities exceeding  $10 \text{ mS}\cdot\text{cm}^{-1}$ . Analogous materials have also been synthesised with  $\text{Na}^+$  as the mobile cation making them attractive for Na-ion solid-state battery applications as well. However, challenges remain, for example, their poor reduction stabilities necessitate additional separator layers when used with metal anodes. In this perspective, an overview is provided of the known compositions, their structures, stabilities, syntheses, and their suggested conduction mechanisms, with an outlook into what developments are needed to see their adoption into solid-state batteries. A comparison will be made between the  $\text{LiMOCl}_4$  and  $\text{NaMOCl}_4$  materials, highlighting the experimental and theoretical challenges when working with this class of materials. While these oxyhalides are promising for use in solid-state batteries, research in this class of materials is still in its infancy, and further research into understanding their structure, processability in air and with solvents, and their potential usage as cathode coatings needs to be explored in greater depth.

employed is susceptible to ignition.<sup>[2]</sup> By replacing the liquid electrolyte with a non-flammable solid one, all-solid-state-batteries have the potential to offer further increased energy and power densities, e.g., by enabling the use of Li metal anodes.<sup>[3]</sup> While solid electrolytes have shown promise, challenges remain in discovering materials with sufficiently high ionic conductivities, redox stabilities, and chemical stability toward moisture, air, solvents and active electrode materials.<sup>[4]</sup>

Several classes of solid electrolyte have been investigated for their applications in solid-state batteries. Of which, different halide solid electrolytes have been of recent interest due to their wide electrochemical stability windows,<sup>[5]</sup> cost-effectiveness,<sup>[6,7]</sup> and ease of production.<sup>[8]</sup> However, the ionic conductivities of halide solid electrolytes are generally low (in comparison to, for example, sulphide solid electrolytes<sup>[9]</sup>) as the close packed  $\text{Cl}^-$  frameworks result in high-energy trigonal coordination pathways that are not conducive for fast ionic conductivities.<sup>[10,11]</sup> This has made it difficult to achieve the  $10 \text{ mS}\cdot\text{cm}^{-1}$  threshold required for high power-density cells using halide solid electrolytes in composite cathodes.<sup>[4]</sup>

## 1. Introduction

As the demand for renewable energy sources has grown, so has the requirement for safe energy storage solutions.<sup>[1]</sup> Conventional Li-ion batteries currently offer high volumetric and gravimetric capacities; however, the flammable liquid electrolyte

J. A. Newnham  
Advanced Centre for Energy and Sustainability  
Department of Chemistry  
School of Natural and Computing Sciences  
University of Aberdeen  
Aberdeen AB24 3UE, UK  
E-mail: [jon.newnham@abdn.ac.uk](mailto:jon.newnham@abdn.ac.uk)

A. G. Squires, D. O. Scanlon  
School of Chemistry  
University of Birmingham Edgbaston  
Birmingham B15 2TT, UK

 The ORCID identification number(s) for the author(s) of this article can be found under <https://doi.org/10.1002/aenm.202504067>

© 2025 The Author(s). Advanced Energy Materials published by Wiley-VCH GmbH. This is an open access article under the terms of the [Creative Commons Attribution](#) License, which permits use, distribution and reproduction in any medium, provided the original work is properly cited.

DOI: 10.1002/aenm.202504067

M. A. Kraft, W. G. Zeier  
Institute of Inorganic and Analytical Chemistry  
University of Münster  
48149 Münster, Germany  
E-mail: [wzeier@uni-muenster.de](mailto:wzeier@uni-muenster.de)

W. G. Zeier  
Forschungszentrum Jülich GmbH  
Institute of Energy Materials and Devices Helmholtz-Institute Münster (IMD-4)  
52425 Jülich, Germany

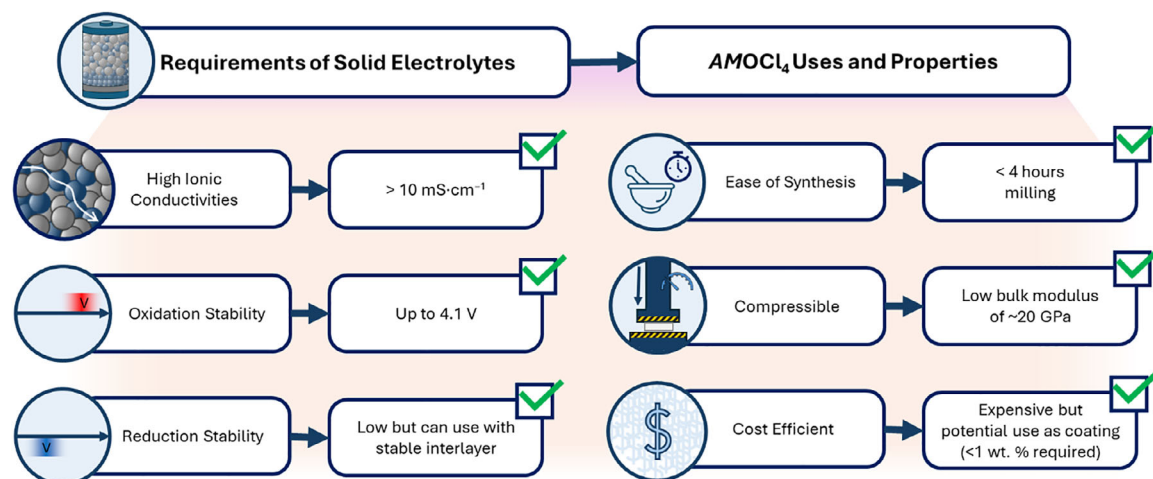


**Figure 1.** Requirements for solid electrolytes and how  $\text{AMOCl}_4$  materials might be used to meet them in all solid-state batteries.

By incorporating oxygen into the halide anion lattice, it has been possible to form non-close packed (oxy)halides with vastly improved ionic conductivities. Notably, the  $\text{LiMOCl}_4$  ( $M = \text{Ta}, \text{Nb}$ ) class has demonstrated ionic conductivities exceeding  $10 \text{ mS}\cdot\text{cm}^{-1}$ , matching that of some liquid electrolytes.<sup>[12]</sup> These materials represent an attractive new direction for solid electrolyte research as they mitigate one of the key issues inhibiting the commercialisation of solid-state batteries with halide solid electrolytes, namely, their often-poor ionic conductivities. These new materials have also been synthesised with  $\text{Na}^+$  as the mobile cation ( $\text{NaNbOCl}_4$  and  $\text{NaTaOCl}_4$ ) which also have high ionic conductivities in the  $\text{mS}\cdot\text{cm}^{-1}$  range<sup>[13,14]</sup> making these oxyhalides attractive for post-lithium-ion batteries as well.<sup>[15]</sup> **Figure 1** outlines some of the key requirements of solid-state electrolytes and how the  $\text{AMOCl}_4$  materials might be used to meet them.

Despite these benefits, several challenges remain with  $\text{AMOCl}_4$  solid electrolytes including their poor reduction stabilities in addition to several current unknowns such as their processability in air or with solvents. Unfortunately, these challenges may also be difficult to address as obtaining an all-encompassing description of these materials is tricky as much about them is still unknown. One of the challenges that makes these materials hard to pin down is their structure as, in the case of  $\text{LiNbOCl}_4$ , three have been proposed thus far – something that will be discussed in detail below. In addition, there seems to always exist a mixture of an amorphous and (semi-)crystalline product with varying coherence lengths and, currently, the relative contributions of these factions toward the overall properties of the material remains unknown.<sup>[16]</sup> This makes studying this class of material challenging as, for example, when changes are made to the composition, it may be difficult to establish how these changes are distributed across the different fractions of the product. This uncertainty also propagates into atomistic simulations because, as the predicted properties are a direct result of the typically small-box used for the simulation, it needs to be considered which structure is used in the calculations, how different fractions of the material interact with each other, and which modelling approaches should be used/developed for crystalline, glassy and glass-ceramic mate-

rials. This also has implications for their adoption as, if the crystalline and amorphous fractions have significantly different electrochemical and mechanical properties, the weight fractions of each will need to be optimised and their interactions understood.

The electrochemical properties of  $\text{AMOCl}_4$  ( $A = \text{Li}, \text{Na}; M = \text{Nb}, \text{Ta}$ ) solid electrolytes make them viable candidates for adoption into commercial all-solid-state-batteries. However, the additional complexities that surround them provide a multitude of challenges that first need to be addressed. In addition, much is still unknown, particularly the  $A = \text{Na}^+$  materials, making them ripe for further study. One such challenge is the cost of the  $M^{5+}$  cation, which would significantly inhibit their commercial adoption. However, to effectively substitute these cations (or to design new materials without them) without also significantly inhibiting the electrochemical properties, a detailed understanding of why these materials behave in the ways they do needs to be obtained.

Therefore, starting with the  $A = \text{Li}^+$  materials (as these are slightly better understood), this perspective aims to provide a discussion of different aspects of  $\text{AMOCl}_4$  solid electrolytes including their synthesis, structure, electrochemistry and stability, and highlight how each of these properties may contribute toward or hinder their efficacy in all-solid-state batteries. To overcome many of these challenges, and to enable their rapid development and validate experimental findings, a strong theoretical understanding is also needed. However, the same challenges listed above, particularly regarding their glass and glass-ceramic behaviour, impede standard modelling approaches for solid electrolyte materials. As such, we further provide a perspective on the challenges of modelling these compounds and potential avenues toward gaining a better theoretical understanding. Finally, we will give focus to what advancements and new understandings would be required to see the adoption of  $\text{AMOCl}_4$  materials into commercial all-solid-state batteries.

## 2. On the Challenge of Establishing the Structure

The structural arrangements of the cations and anions in the  $\text{LiMOCl}_4$  ( $M = \text{Nb}^{5+}, \text{Ta}^{5+}$ ) materials are somewhat ambiguous as the powder diffraction patterns of these materials are

difficult to interpret due to broad and low intensity reflections. While the structures of the  $\text{LiMOCl}_4$  materials are somewhat debatable, pragmatically, the crystal structure of a solid electrolyte does not matter so long as they perform well in cells. However, it does become an issue when trying to explain structure-property relationships as it inhibits a fundamental understanding of why these materials behave in the ways that they do. Without it, our abilities to make informed decisions on how these materials can be further optimised or how we can design other materials with similar properties are also restricted. With  $\text{LiMOCl}_4$  in particular, the existence of (semi-)crystalline fractions that are embedded in an amorphous matrix further increases the difficulty in tracking how changes to stoichiometry or synthesis can influence the structure and properties of the material as it may be unknown how those changes are distributed across the different fractions.<sup>[16]</sup>

These difficulties in studying the crystal structures originate from short coherence lengths and high strains present that form as a result of the required mechanochemical synthesis procedures, which are retained even after subsequent annealing.<sup>[17,18]</sup> Despite attempts to optimise the annealing conditions, it has not yet been possible to synthesise these compounds with larger coherence lengths, possibly because the oxyhalides are metastable with formation energies that are  $\sim 19$  meV/atom above the convex hull.<sup>[19]</sup> As such, annealing temperatures are limited to a maximum of  $\approx 150$  °C for  $\text{LiNbOCl}_4$  else it decomposes to form  $\text{LiCl}$ ,  $\text{Nb}_2\text{O}_5$ , and  $\text{NbOCl}_3$ ,<sup>[17,20]</sup> although  $\text{LiTaOCl}_4$  has a slightly higher thermal stability having previously been annealed at 300 °C.<sup>[12]</sup> Directly after milling some Bragg peaks are visible for  $\text{LiNbOCl}_4$ , whereas  $\text{LiTaOCl}_4$  is fully amorphous. However, after heating the milled products at 100 and 300 °C, respectively, there does not appear to be any significant difference in crystallinities between the two materials – although this has not yet been confirmed.<sup>[12]</sup>

Much of the research into the structure has focused on  $\text{LiNbOCl}_4$ , which is likely due to the lower cost of Nb relative to Ta, and it more readily crystallising relative to  $\text{LiTaOCl}_4$ . Here, it is generally agreed that the incorporation of  $\text{O}^{2-}$  into crystalline  $\text{LiNbCl}_6$  breaks the hexagonal close packing of  $\text{Cl}^-$  anions<sup>[21]</sup> resulting in the formation of 1D  $[\text{NbOCl}_4]_{\infty}^-$  chains of trans- $[\text{NbO}_2\text{Cl}_4]^{3-}$  octahedra that are apex sharing at the  $\text{O}^{2-}$  anion, and these chains are then surrounded by various  $\text{Li}^+$  cation sites. It is first important to note that, when discussing the structure of  $\text{LiMOCl}_4$ , it is necessary to distinguish between whether one is referring to the local or long-range structure. This is important as the  $[\text{MO}_2\text{Cl}_4]^{3-}$  octahedra are highly deformable with dynamic rotational disorder,<sup>[17,18]</sup> meaning that there seem to be varying (and random) dihedral angles between adjacent octahedra along the  $[\text{MOCl}_4]_{\infty}^-$  chains.

This fact is important to consider, as differences in the terminal  $\text{Cl}^-$  positions and  $M\text{—Cl}$  bond lengths on these chains need to be accounted for in models of the local structure, but the in the long-range, space- and time-averaged models (such as those determined by powder diffraction), rotations and deformations of the  $[\text{MO}_2\text{Cl}_4]^{3-}$  octahedra can equalise the “observed” bond lengths and atomic positions. Considering this distinction, three different structure models have been proposed thus far for  $\text{LiNbOCl}_4$ , which can be split into two categories based on whether they describe local or long-range structure data (Figure 2). These structures potentially also apply to  $\text{LiTaOCl}_4$ ,

however, the same in-depth analysis has not yet been performed on this material.

For the long-range structure describing the Bragg data,  $\text{LiNbOCl}_4$  was first proposed to crystallise in  $Cmc2_1$  based on substitutions in the computationally predicted phase,  $\text{LiVOF}_4$ .<sup>[12]</sup> However, this structure model results in many of the expected Bragg peaks showing zero intensity indicating the need for a higher symmetry model.<sup>[18]</sup> In addition, it was noted that the  $Cmc2_1$  structure model contains Nb—Cl bond lengths that range considerably from 1.96 to 3.00 Å, whereas  $\text{TiNbOCl}_4$  (with similar 1D  $[\text{NbOCl}_4]_{\infty}^-$  chains) contains a tight range of Nb—Cl bond lengths from 2.38 to 2.41 Å.<sup>[22]</sup>

As such, this model was later refined to a higher symmetry  $I4/m$  structure model based on more plausible bond chemistries.<sup>[18]</sup> Here, in an attempt to construct a long-range structural model that was more compatible with the observed superionic conductivity, the  $I4/m$  model was refined with three partially occupied  $\text{Li}^+$  positions, which were determined based on global stability index calculations.<sup>[18]</sup> However, these  $\text{Li}^+$  positions were later determined experimentally based on co-refinements against X-ray and neutron diffraction data.<sup>[16]</sup> In these co-refinements, to better fit the data with fewer unphysical parameters, the authors also split  $\text{Nb}^{5+}$  site to account for the different expected Nb—O bond lengths observed in the local structure (which is discussed below). The  $I4/m$  long range structure model is supported by the fact that  $\text{LiNbOCl}_4$  does not give a Second Harmonic Generation (SHG) signal indicating that it is indeed centrosymmetric on large length scales.<sup>[16]</sup> While the  $I4/m$  long-range structure model does improve upon the fit of powder diffraction data of  $\text{LiNbOCl}_4$ , it cannot be used to model the local structure as multiple Nb—Cl and Nb—O bond lengths are observed in the X-ray Pair Distribution Function ( $G(r)$ , PDF).<sup>[17]</sup> In addition, it also does not effectively account for the expectation of second order Jahn-Teller (SOJT) distortions associated with the  $\text{Nb}^{5+}$  cation. To account for these factors, a  $Cc$  structure model was proposed for the local structure of  $\text{LiNbOCl}_4$ .<sup>[17]</sup> As such, the  $I4/m$  model can be used to describe the long-range structure of  $\text{LiNbOCl}_4$ , and  $Cc$  the local structure.

Although both the  $I4/m$  and  $Cc$  structure models can be used to somewhat adequately fit the diffraction data of  $\text{LiNbOCl}_4$ , respectively, it would be hasty to describe either as the definitive long-range or local structures, as there are still uncertainties associated with both. For example, in co-refinements of the X-ray and neutron diffraction data of  $\text{LiNbOCl}_4$ , it was still found that it was not possible to obtain physical atomic displacement parameters for  $\text{O}^{2-}$  using the  $I4/m$  model for the long-range structure, which likely reflects the fact that  $\text{Nb}^{5+}$  will not safely sit in the centre of the  $[\text{NbO}_2\text{Cl}_4]^{3-}$  octahedra on a local scale. Whereas one would expect to observe one long and one short Nb—O bond, and O—Nb—O bond angles that are not 180°-similar to what is observed in other oxychlorides such as  $\text{NbOCl}_3$ ,<sup>[23]</sup> and  $\text{TiNbOCl}_4$ .<sup>[22]</sup> Similarly, the  $Cc$  model of the local structure can be used to adequately fit the  $G(r)$  of  $\text{LiNbOCl}_4$  without the need for any unphysical parameters, and is supported by density functional theory based structural relaxation and a calculated phonon dispersions without imaginary modes.<sup>[17]</sup> However, it was also shown that  $\text{LiNbOCl}_4$  contains a mixture of amorphous and (semi-)crystalline fractions and it is unknown how these contribute to the overall  $G(r)$ .<sup>[16]</sup> As such, care needs to be taken to

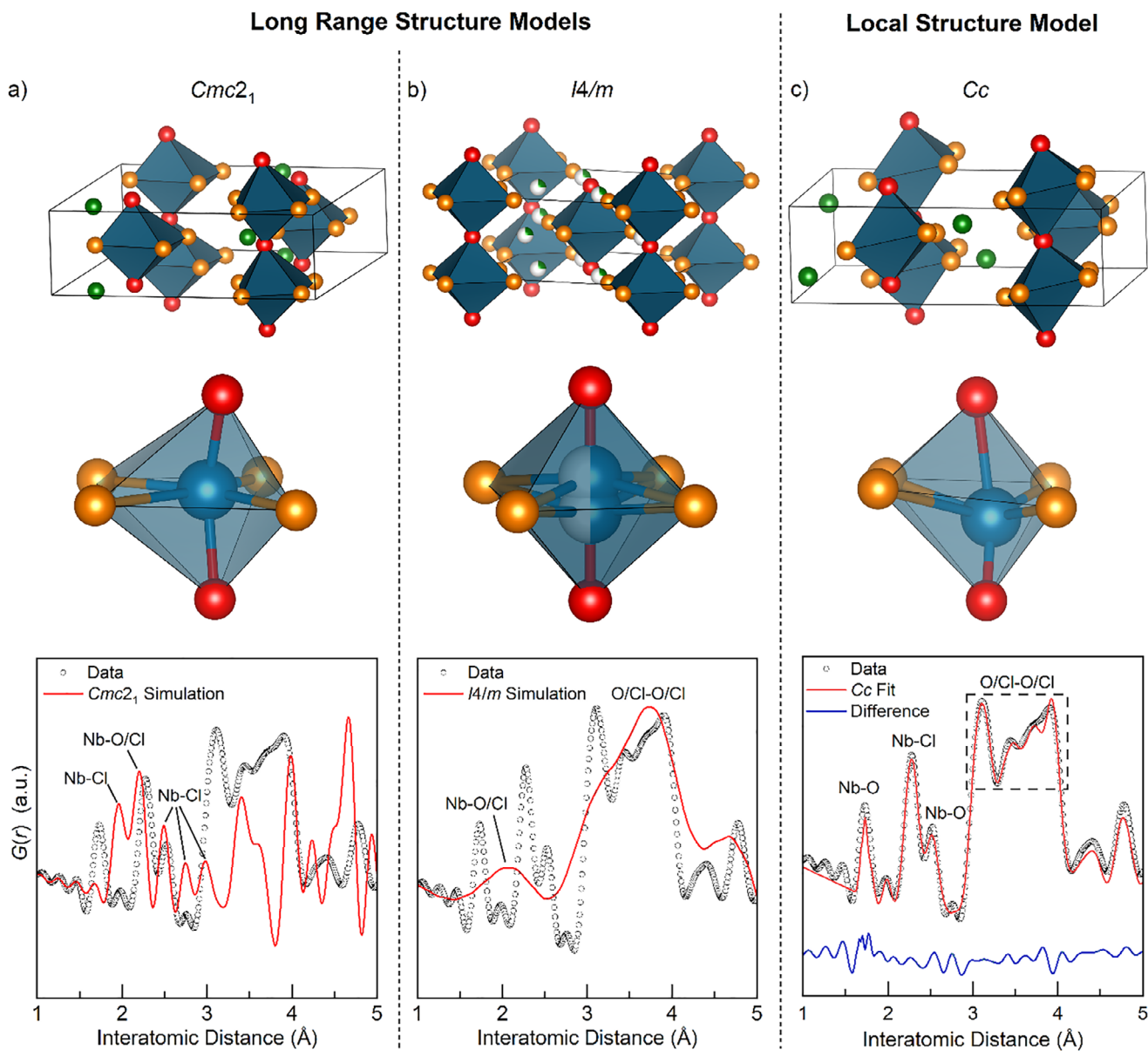


**Figure 2.** The proposed structures of  $\text{LiNbOCl}_4$  and their simulated  $G(r)$  data using each model. a) First, in space group  $Cmc2_1$ <sup>[12]</sup> constructed based on  $\text{Nb}^{5+}$ -for- $\text{V}^{5+}$  and  $\text{Cl}^-$ -for- $\text{F}^-$  substitutions in the hypothetical material,  $\text{LiVOF}_4$ , and b) second in space group  $I4/m$ , which was later proposed based on more plausible bond chemistries.<sup>[18]</sup> The  $\text{Li}^+$  positions in the  $I4/m$  model were first determined based on global stability index calculations but are shown here using  $\text{Li}^+$  positions determined from refinements of neutron diffraction data.<sup>[16]</sup> c) A local structural model of  $\text{LiNbOCl}_4$  in  $Cc$  was later proposed based on the observation of multiple Nb–Cl and Nb–O bond lengths in the PDF of the material.<sup>[17]</sup> Structures and fits were redrawn from data in refs. [12] and [16].

ensure that the  $Cc$  model does not fit the local structure of  $\text{LiNbOCl}_4$  better solely due to there being more open parameters.

In addition, it was also shown that  $\text{LiNbOCl}_4$  contains substitutional disorder of the  $\text{O}^{2-}$  and  $\text{Cl}^-$  anions at the bridging site between  $[\text{NbO}_2\text{Cl}_4]^{3-}$  octahedra that had not been accounted for in any model of the local or long-range structures.<sup>[16]</sup> This substitutional disorder on the bridging anion site in these chains is somewhat unexpected considering the considerably different ionic radii, polarizability, and charges of the  $\text{O}^{2-}$  and  $\text{Cl}^-$  anions, which is likely why it was overlooked in structural models de-

scribed above. This structural disorder likely originates from the high energy ball-milling resulting in the kinetic stabilisation of these substitutions, which is similarly observed in  $X^-/\text{S}^{2-}$  disorder in Li-argyrodites upon heating.<sup>[24]</sup>

The existence of the anionic substitutional disorder is important to consider in these materials as it was shown that the anion ratio is proportional to the coherence length of the crystalline fraction in  $\text{Li}_{1-x}\text{NbO}_{1-x}\text{Cl}_{4+x}$ , which in turn affects the obtainable ionic conductivities.<sup>[16]</sup> Here, it was proposed that this proportionality exists as the  $\text{O}^{2-}$  anions cannot occupy the terminal

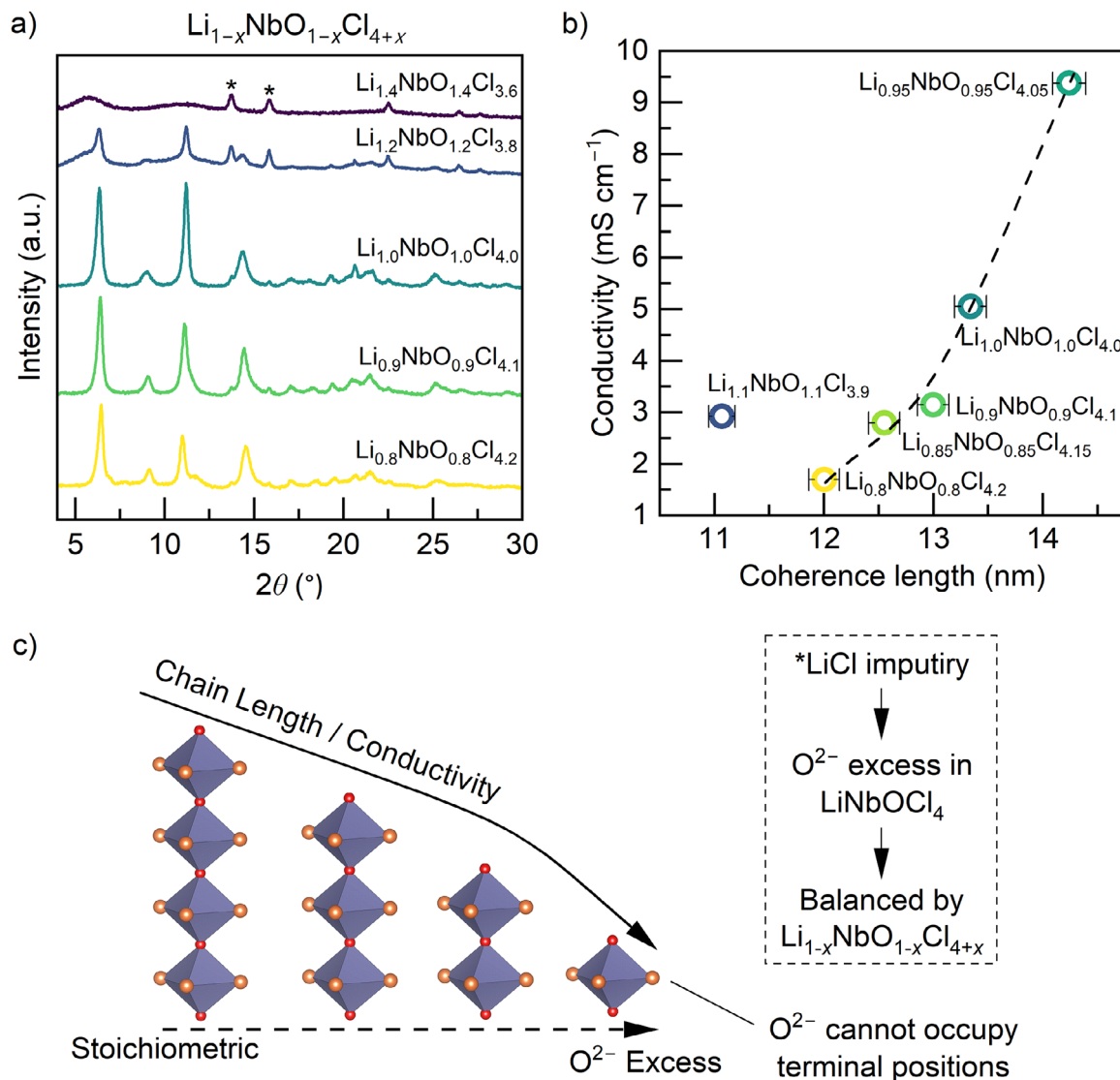


**Figure 3.** a) Diffraction patterns of  $\text{Li}_{1-x}\text{NbO}_{1-x}\text{Cl}_{4+x}$  highlighting how they correlate with the  $\text{Li}^+$  content and anion ratio (redrawn from ref. [16]). The asterisks highlight the reflections associated with LiCl. b) The ionic conductivities of  $\text{Li}_{1-x}\text{NbO}_{1-x}\text{Cl}_{4+x}$  materials highlighting how they correlate with the obtained coherence lengths. c) A schematic showing how an  $\text{O}^{2-}$  excess in  $\text{LiNbOCl}_4$  may lead to shortened chain lengths as it cannot occupy the terminal sites of the  $[\text{NbOCl}_4]_{\infty}^-$  chains.

$\text{Cl}^-$  sites of the chains and was evidenced by the absence of the expected peak at  $\approx 1000 \text{ cm}^{-1}$  in the Raman spectra, even in samples that were made  $\text{O}^{2-}$  rich. Therefore, any excess of  $\text{O}^{2-}$  results in a disruption to the overall chain length (Figure 3) potentially leading to a breaking of those chains and amorphization. This trend in the conductivity and crystallinity has also been observed in other reports of  $\text{LiNbOCl}_4$  where controlling the annealing conditions results in improved crystallinities and therefore higher ionic conductivities.<sup>[12,17]</sup> This however is not the case for all halide solid electrolytes as, for example, the ionic conductivity of amorphous  $\text{LiTaCl}_6$  is six orders of magnitude greater than when it is fully crystallised.<sup>[21,25]</sup>

The existence of second order Jahn-Teller distortions may also affect the obtained ionic conductivity in these materials. For example,  $\text{NaTaCl}_6$  exhibits a  $P2_1/c$  structure<sup>[26]</sup> with distorted

$[\text{TaCl}_6]^-$  octahedra in comparison to the higher symmetry  $P4_2/m$   $\text{NaSbCl}_6$ <sup>[27]</sup> material with no expressed SOJT distortions. This is important to consider as the distorted octahedra in  $\text{NaTaCl}_6$  also results in a different ordering of the mobile  $\text{Na}^+$  cations. As such, it is currently unknown how the SOJT distortions of the  $[\text{MO}_2\text{Cl}_4]^{3-}$  affects the  $\text{Li}^+$  positions in the  $\text{LiMOCl}_4$  materials, and therefore their mobilities and ionic conductivities.

It is important that the structures of both  $\text{LiMOCl}_4$  materials are carefully determined. However, to achieve this, several considerations need to be made. First, routes toward fully crystallising these materials need to be demonstrated so that the structure and properties of the crystalline fraction can be disambiguated from the amorphous matrix. This is important as, while it is known that the ionic conductivity is proportional to the coherence length in these materials,<sup>[16]</sup> it is unknown exactly why and

to what extent the transport properties vary in different fractions of the material. It would also allow for any structural modifications to be tracked when doping the material as it is currently unknown how any compositional changes may be distributed across different fractions of the product. In addition, when synthesising  $\text{LiMOCl}_4$  from  $\text{LiOH}$  and  $\text{MCl}_5$ , care needs to be made to ensure that there are no protons in the materials that could influence the obtained structure or conductivities via  $^1\text{H}$  NMR (Nuclear Magnetic Resonance). After these considerations, both the local and long-range structures of  $\text{LiMOCl}_4$  will need to be carefully re-established using a combination of both diffraction and spectroscopic techniques, as well as theoretical studies into the energies and stabilities of those structures. Here, the use of neutron-based techniques at low temperatures is especially important to track the positions and occupations of the light  $\text{Li}^+$  and  $\text{O}^{2-}$  ions.

Finally, we emphasise that care must be taken when selecting a structural model of  $\text{LiMOCl}_4$  for refinements and simulations, and the limitations of each model for analysing different data sets should be carefully assessed. For example, understanding if a measurement technique is probing the average long-range structure (e.g., X-ray/neutron diffraction and SHG) or the average local structure (e.g., Raman spectroscopy, NMR spectroscopy, extended X-ray absorption fine structure (EXAFS) spectroscopy, and pair distribution functions). It should also be noted that, while these models have been studied for the structure of  $\text{LiNbOCl}_4$ , they may not necessarily apply to  $\text{LiMOCl}_4$  materials where  $M$  is a metal that does not exhibit a second order Jahn-Teller distortion.<sup>[28]</sup> As such, the structure remains an important aspect of this class of materials that is yet to be fully understood, and research efforts into new synthetic routes toward highly crystalline  $\text{LiMOCl}_4$  materials (discussed in more detail later) are still highly important.

### 3. Computational Exploration of Glass-Ceramic Oxhalides

Computational methods are powerful complements to experimental techniques when studying complex electrolyte materials such as the  $\text{AMOCl}_4$  family, capable of validating experimental observations,<sup>[24]</sup> guiding rational doping strategies,<sup>[29]</sup> and elucidating intricate structure-property relationships<sup>[30]</sup> that are otherwise inaccessible by experiments alone. Despite these motivations, the glass-ceramic or semi-crystalline nature of the various  $\text{AMOCl}_4$  materials make them inherently challenging to study using standard atomistic simulation methods. In non- or semi-crystalline solid electrolytes, the absence of long-range periodicity undermines the applicability of conventional first principles materials modelling techniques, which typically rely on periodic boundary conditions to model a small, representative unit of an extended crystalline lattice.

In ordered crystalline materials, observables can often be accurately predicted by sampling the ground state structure alone, since it dominates the thermodynamic ensemble that describes the real-world behaviour of the material due to its low energy and symmetry-constrained degeneracy. However, in disordered or amorphous systems, no single small-box structure is likely to meaningfully represent the full thermodynamic ensemble. Observables can instead be modelled as ensemble averages over

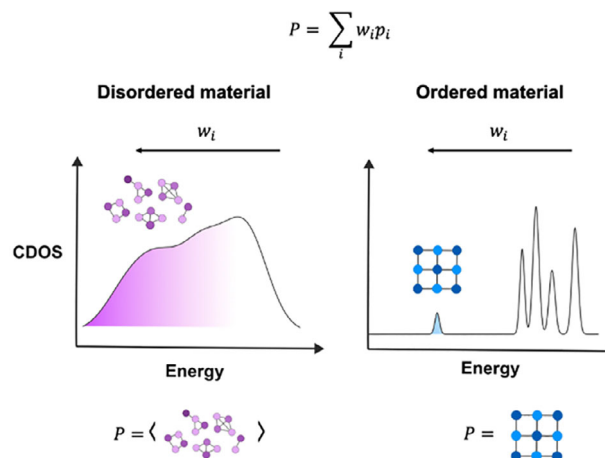


**Figure 4.** Comparing the configurational density of states and modelling approaches of disordered and ordered materials. For both cases, the observable property  $P$  is a weighted average of all the microstates in the ensemble of each material. For the ordered material only the ground state has a significant Boltzmann weighting, for the disordered material, an ensemble of states needs to be sampled to derive an accurate average.

a distribution of microstates, each weighted by its Boltzmann factor,<sup>[31,32]</sup> as illustrated in **Figure 4**. Recent density functional theory (DFT) studies on  $\text{LiMOCl}_4$  compounds have revealed that many proposed structural variants differ in energy by only a few meV per atom – less than the thermal energy at room temperature ( $\approx 25$  meV).<sup>[19]</sup> These small energy differences imply that multiple distinct configurations are thermally accessible, and may all need to be considered to obtain a comprehensive understanding of atomistic structure-property relationships in these systems.

There are not just multiple structural microstates to consider in  $\text{AMOCl}_4$ , but also significant vibrational and rotational disorder. Capturing this dynamic disorder requires simulation times sufficiently long to resolve structural rearrangements, and timescales typically sufficient for sampling ion transport (e.g.,  $\text{Li}^+$  or  $\text{Na}^+$  diffusion) in rigid frameworks may be too short to sample relevant structural fluctuations in dynamically evolving frameworks. Short or single-trajectory simulations therefore risk underestimating lattice flexibility and overlooking transient structural configurations that contribute to vibrational properties. Accurate characterisation therefore demands both extended simulations and ensemble averaging across structurally distinct trajectories, capturing both thermally accessible structural states and their time-dependent evolution.

While ensemble sampling is essential for capturing functional properties, it also challenges the use of single-structure formation energies as proxies for thermodynamic stability. In ordered materials, this metric can be meaningful, as a single structure dominates the finite-temperature ensemble. But in disordered materials, the actual thermodynamic state is distributed across many low-energy configurations. The energy above hull calculated from any one structure is therefore highly sensitive to which minimum is chosen and may not meaningfully reflect the stabilisation observed experimentally, either because there is no synthetic route to isolate purely the ground state structure, but in addition such calculations tend to omit entropic contributions. For

example, vibrational and configurational entropy can be substantial in solid electrolytes with disordered or flexible frameworks, and can stabilise materials at finite temperature that would appear thermodynamically or dynamically unstable at 0 K.<sup>[33,34]</sup>

Taken together, these limitations illustrate that the combination of a single static configuration and a zero-temperature framework makes it especially problematic to rely on single-structure energetics when modelling disordered materials like  $\text{AMoCl}_4$ . Without incorporating thermal effects and ensemble averaging, formation energies and hull distances risk misrepresenting both the stability and functional behaviour of real materials. Predictive modelling of such systems must move beyond conventional approaches, adopting ensemble-based frameworks that account for configurational diversity, thermal accessibility, and the statistical nature of the structure–property landscape.

Two practical strategies are commonly used to generate such ensembles. The first is a hypothesis-driven approach that incorporates known local structural features (such as coordination geometries or motifs inferred from spectroscopy or total scattering) into initial configurations.<sup>[35]</sup> This is effective when the form of disorder is relatively well constrained. Such structures could be used for example, to investigate the local structure around anion-substitutional defects in  $\text{LiNbOCl}_4$ .<sup>[16]</sup> The second approach involves attempts at a first-principles derivation of representative structures (or an ensemble of structures). This has involved using techniques such as melt–quench molecular dynamics<sup>[36,37]</sup> – an approach recently taken to study dynamics in  $x\text{Na}_2\text{O}\text{-TaCl}_5$  glass electrolytes<sup>[30]</sup> – structure enumeration<sup>[37]</sup> or statistical-mechanical models<sup>[38]</sup> to produce disordered models that are consistent with known chemistry and (once suitably averaged) can be used to assist in the interpretation of experimental data. Because constructing and sampling sufficiently large ensembles is often computationally demanding (especially at the DFT level) lower-cost models such as classical potentials<sup>[39]</sup> or, increasingly, machine-learned interatomic potentials are used to access longer timescales and larger supercells.

These approaches are often complementary: motif-based models can be used as starting points for further sampling, while statistically averaged structures may help refine or constrain structural hypotheses. In systems like  $\text{AMoCl}_4$ , where both static and dynamic disorder are relevant, and where experimental measurements reflect ensemble behaviour, a combination of these strategies is typically required. Moreover, computed quantities such as structure factors, vibrational densities of states, and diffusion coefficients depend sensitively on the underlying ensemble. As such, computing the properties and structure-property relationships in  $\text{AMoCl}_4$  materials requires consideration of how accurately the simulated ensemble represents the as-synthesised material.

#### 4. Tentative Structure-Property Relationships

Gaining an understanding how the  $\text{Li}^+$  conductivity in  $\text{LiMoCl}_4$  materials is influenced by the – potentially vibrationally and rotationally disordered –  $[\text{MOCl}_4]_{\infty}^-$  chains is highly valuable as it allows us to design and identify other materials with high ionic conductivities based on their structural motifs. It would also allow us to efficiently optimise the ionic conductivities of these materials based on informed doping strategies.

Halide solid electrolytes such as  $\text{Li}_3\text{InCl}_6$ <sup>[40]</sup> and  $\text{Li}_2\text{ZrCl}_6$ <sup>[41]</sup> have higher  $\text{Li}$ -ion densities than what is found in  $\text{LiMoCl}_4$ . Despite this, the  $\text{LiMoCl}_4$  materials still have far higher ionic conductivities. Considering their low mobile ion concentrations, this indicates that these materials also have extremely high ionic mobilities (Figure 5a).<sup>[4]</sup> This is important as it has previously been estimated that  $\approx 40\%$  of the  $\text{Li}^+$  in a solid-state battery is being used up in the solid electrolyte rather than contributing toward the capacity.<sup>[4]</sup> Therefore, having electrolytes with low  $\text{Li}^+$  densities is advantageous for minimising costs. However, it should be noted that the cost of the metal cation is also significant in the case of the  $\text{LiMoCl}_4$  materials. Nevertheless, by studying the  $\text{LiMoCl}_4$  class of materials and developing an understanding of what makes their mobilities so high can help us to design and identify other high-performance and cost-effective solid electrolytes.

Clearly, to ascertain structure-property relationships in  $\text{LiMoCl}_4$  materials, their structures need to be better understood. This includes gaining a comprehensive understanding of the local and long-range structures, as well as an understanding of the vibrational and rotational disorder present in these systems. While each of the three proposed structure models could be used to fit the diffraction data, it would be problematic to use any of these alone to obtain structure-property relationships as they are static models and therefore do not incorporate the vibrational or rotational disorder needed to study  $\text{Li}^+$  migration. Therefore extended simulations and ensemble averaging are required. Nevertheless, while the crystal structure for the  $\text{LiMoCl}_4$  materials may yet need to be more specified, the 1D  $[\text{MOCl}_4]_{\infty}^-$  chains certainly are a part of it and are thought to influence the mobile ion migration in three main ways, as depicted in Figure 5.

First, Jun et. al. studied diffusion processes in  $\text{LiNbOCl}_4$  using ab initio molecular dynamics (AIMD) and the difference in probability between an  $[\text{NbO}_2\text{Cl}_4]^{3-}$  octahedral rotation along the  $z$  axis and the  $\text{Li}^+$  ions either hopping or not hopping.<sup>[19]</sup> In doing so, they found that the tilting ( $< 30^\circ$ ) of the individual octahedra in the  $[\text{MOCl}_4]_{\infty}^-$  chains allows for the correlated hopping of  $\text{Li}^+$  ions through the soft-cradle effect resulting in an optimised energy landscape for  $\text{Li}^+$  migration.

Second, it was also observed through AIMD simulations that there are large variations in the inter-chain distances as a result of a low chain rigidity in  $\text{LiNbOCl}_4$ , which was supported by the low calculated bulk modulus of 22.7 GPa indicating the relatively ductile nature of the material.<sup>[17]</sup> This, along with the deformable  $[\text{NbO}_2\text{Cl}_4]^{3-}$  octahedra, results in flexible  $[\text{NbOCl}_4]_{\infty}^-$  chains that stabilise different  $\text{Li}^+$  positions which further flattens the energy landscape for  $\text{Li}$ -ion migration.

Third, in addition to there being a flat energy landscape, there is little in the  $\text{LiMoCl}_4$  structure that can impede the migration of  $\text{Li}^+$  ions. For example, through bond valence sum energy (BVSE) calculations, it has been shown that, due to the 1D nature of the  $[\text{NbOCl}_4]_{\infty}^-$  chains, the  $\text{Li}^+$  ions can move parallel to the chains with activation energies as low as 0.04 eV (Figure 5b,c).<sup>[18]</sup> In addition, it has been proposed that the low spatial density of the  $M^{5+}$  cations results in a decreased likelihood of the migrating  $\text{Li}^+$  ions being repulsed within the diffusion channels.<sup>[19]</sup>

As stated, gaining an understanding how the  $\text{Li}^+$  conductivity in  $\text{LiMoCl}_4$  materials is influenced by the  $[\text{MOCl}_4]_{\infty}^-$  chains is

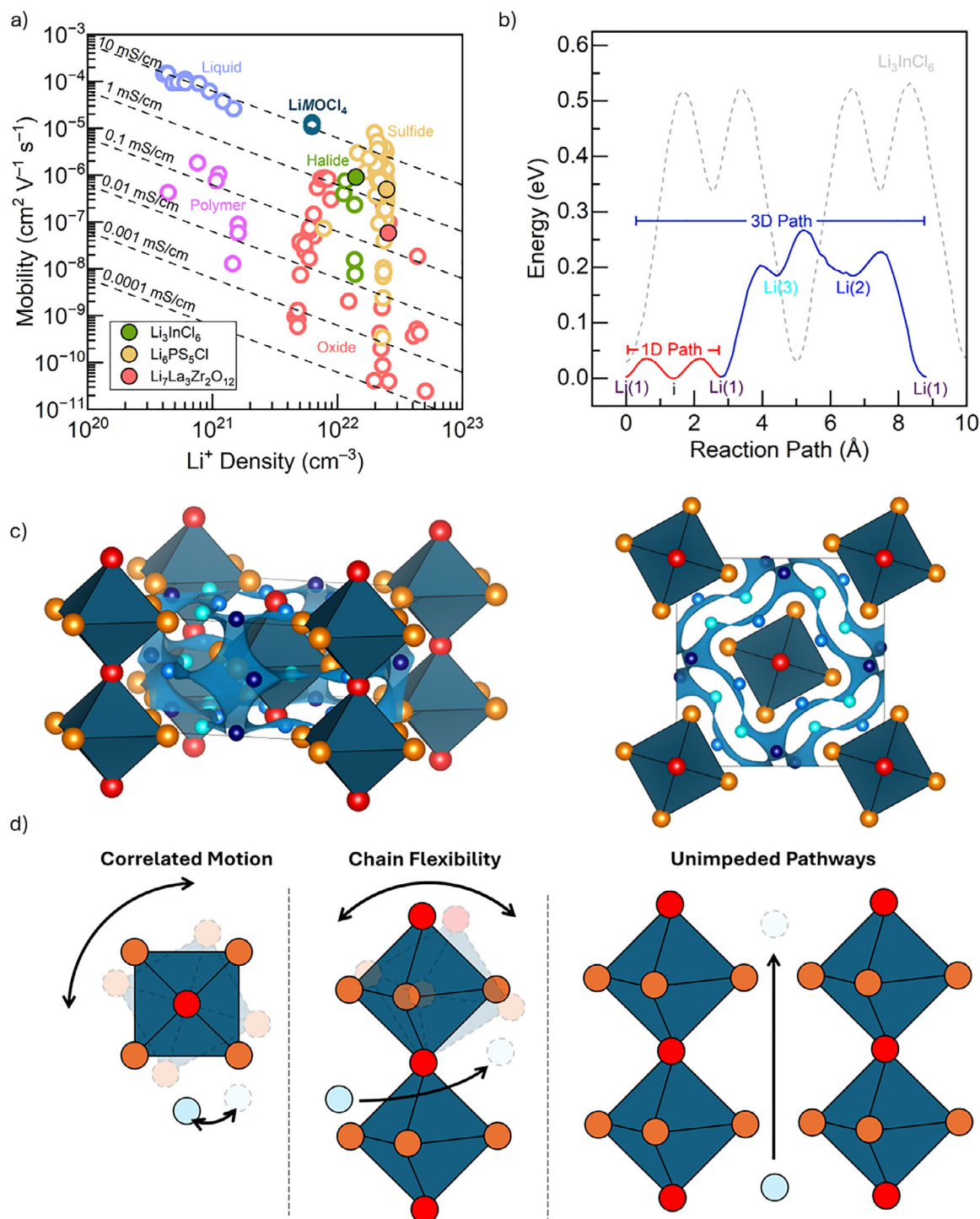


**Figure 5.** a) The ionic conductivity of  $\text{LiMOCl}_4$  in comparison to other classes of solid electrolytes highlighting its high  $\text{Li}^+$  mobility and low  $\text{Li}^+$  carrier density. The data set containing the  $\text{Li}^+$  carrier densities and mobilities of different solid electrolytes was obtained from ref. [4] with supplement from ref. [42]. The mobilities of  $\text{LiMOCl}_4$  were calculated from the ionic conductivities of each material in ref. [12] and the  $\text{Li}^+$  carrier density was calculated from using the Cc local structural model<sup>[17]</sup> of  $\text{LiNbOCl}_4$ . b) Bond valence sum energy (BVSE) model of  $\text{LiNbOCl}_4$ <sup>[18]</sup> showing the low energy barriers for  $\text{Li}^+$  migration along 1D paths (parallel to the  $[\text{MOCl}_4]_{\infty}^-$  chains) in comparison to  $\text{Li}_3\text{InCl}_6$ .<sup>[43]</sup> c) Calculated BVSE isosurfaces showing possible migration pathways in the 14/m long-range structural model. The coloured spheres represent the same  $\text{Li}^+$  sites as in b (recalculated and plotted from the methods in ref. [18]). d) Structure property relationships in  $\text{LiNbOCl}_4$ . The correlated motion of  $[\text{MO}_2\text{Cl}_4]^{3-}$  octahedra and  $\text{Li}^+$  (left), and the flexible  $[\text{MOCl}_4]_{\infty}^-$  chains (center) lead to a flat energy landscape for  $\text{Li}^+$  conduction. Meanwhile, the 1D nature of the  $[\text{MOCl}_4]_{\infty}^-$  chains (right) form unimpeded conduction pathways.

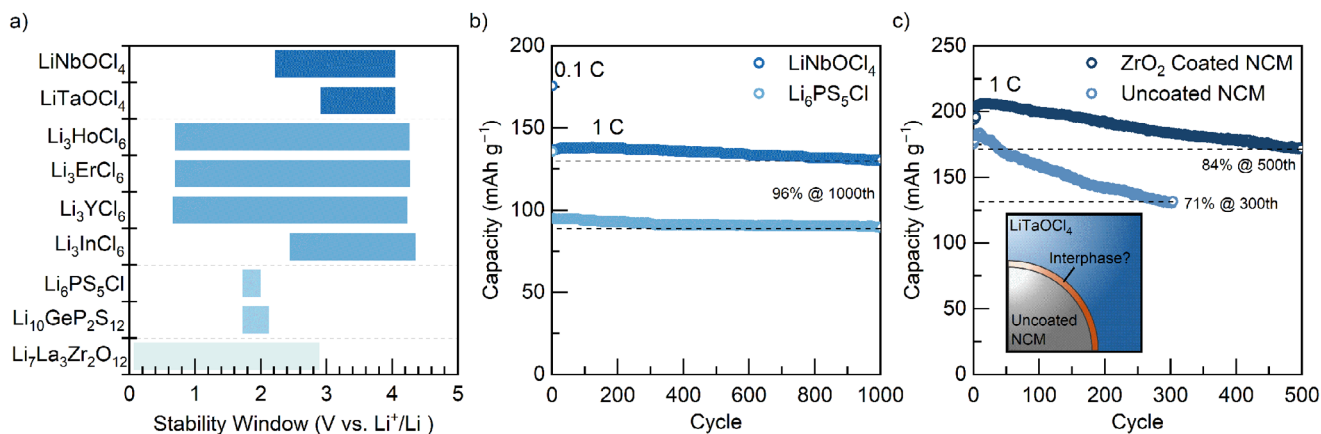


**Figure 6.** a) The calculated electrochemical stability windows of LiNbOCl<sub>4</sub> and LiTaOCl<sub>4</sub><sup>[19]</sup> in comparison to other halide,<sup>[46]</sup> sulfide<sup>[47]</sup> and oxide<sup>[48]</sup> solid electrolytes. b) Capacity retentions of cells containing LiNbOCl<sub>4</sub> and Li<sub>6</sub>PS<sub>5</sub>Cl catholytes with the same LiNi<sub>0.92</sub>Co<sub>0.04</sub>Mn<sub>0.04</sub>O<sub>2</sub> cathode. Data digitised from ref. [20] c) Capacity retentions of cells containing amorphous LiTaOCl<sub>4</sub> catholytes with LiNi<sub>0.9</sub>Co<sub>0.05</sub>Mn<sub>0.05</sub>O<sub>2</sub> (NCM955) cathodes, highlighting the increased capacity retention when a ZrO<sub>2</sub> cathode coating is used. Data digitised from ref. [45].

highly valuable as it allows us to design and identify other materials with high ionic conductivities based on their structural motifs, and to also make informed doping strategies. To achieve this, the LiMOCl<sub>4</sub> materials need to be studied in greater depths than typical “diffraction then impedance” experiments. Before the mechanisms underpinning their high ionic conductivities can meaningfully be deduced, both the local and long-range structures of crystalline and amorphous LiMOCl<sub>4</sub> will need to be carefully re-established using the considerations provided earlier. This will then allow for the structure-property relationships to be examined by studying the movement of Li<sup>+</sup> over various time and length scales using impedance spectroscopy, pulse-field gradient NMR, NMR relaxometry, and quasi-elastic neutron scattering,<sup>[44]</sup> as well as by computational techniques such DFT and ab initio molecular dynamics. To achieve an in-depth understanding of the structure property-relationships in LiMOCl<sub>4</sub>, these materials also need to be substituted, and the influences of those substituents tracked. For example, introducing *M*-cation substitutions that influence the [MOCl<sub>4</sub>]<sub>∞</sub><sup>-</sup> chain rigidity could help to establish the extent to which this structural feature benefits the ionic conductivity.

While this knowledge is highly valuable, we note that, it is likely not the ionic conductivities of the LiMOCl<sub>4</sub> materials that would impede their development into commercial cells. Rather, it is the lacking reduction stabilities, and the costs associated with their production that would limit their adoption. However, an understanding of the structure and structure-property relationships is still needed to overcome these challenges.

## 5. Cell Performance and Redox Stability

In addition to high ionic conductivities, electrolytes require wide voltage windows in which they can operate. Like most halide solid electrolytes, both LiMOCl<sub>4</sub> materials (*M*=Nb and Ta) are predicted to have good oxidation stabilities of up to 4.06 V versus Li<sup>+</sup>/Li,<sup>[19]</sup> which agrees with the experimental value of 4.1 V for LiTaOCl<sub>4</sub>.<sup>[45]</sup> In contrast, the reductive stabilities of the LiMOCl<sub>4</sub> materials are relatively poor as LiNbOCl<sub>4</sub> and LiTaOCl<sub>4</sub> decom-

pose at 2.9 and 2.2 V, respectively, which is associated with the reduction of the M<sup>5+</sup> cation.<sup>[12,19]</sup>

Here, it should be noted that the incorporation of oxygen does not improve the redox stability of the LiMOCl<sub>4</sub> relative to LiMCl<sub>6</sub>, as LiTaCl<sub>6</sub> has a stability window of 2.3–4.4 V.<sup>[25]</sup> Figure 6a shows the calculated stability windows of the LiMOCl<sub>4</sub> materials in comparison to other halide,<sup>[46]</sup> sulfide<sup>[47]</sup> and oxide<sup>[48]</sup> solid electrolytes highlighting their lower reduction stabilities. However, this is not necessarily an issue, depending on the electronic and ionic transport properties of the resulting interphase. For example, while the calculated stability window of the Li<sub>6</sub>PS<sub>5</sub>Cl is quite narrow, in reality it is much wider due to the kinetic stabilisation by the solid electrolyte interphase<sup>[49–51]</sup> (SEI) and hence can be used as an interfacial layer between the halide solid electrolytes and metal/alloy anodes.<sup>[52]</sup> In fact, both sulphide<sup>[20]</sup> and oxide<sup>[53]</sup> solid electrolytes have been used as interlayers between oxyhalide materials and Li/LiIn anodes. Unfortunately, as NaTaOCl<sub>4</sub> forms less ionically conductive interphase between it and Na metal,<sup>[14]</sup> the same is likely true for LiMOCl<sub>4</sub> making them incompatible with Li metal anodes. As such, the LiMOCl<sub>4</sub> materials may effectively be used as catholytes, but not as separators without an additional interlayer.<sup>[52]</sup>

The poorer reduction stabilities of the LiMOCl<sub>4</sub> materials are a general concern associated with halide solid electrolytes (such as Li<sub>3</sub>YCl<sub>6</sub> and Li<sub>3</sub>InCl<sub>6</sub><sup>[54]</sup>) as the requirement of a stable interlayer<sup>[52]</sup> reduces the obtainable volumetric and gravimetric capacities. As such, additional research should be spent on studying their decomposition products and trying to improve the reduction stability of these materials. This also relates back to the need to gain a deeper understanding of the crystal structure in these materials as a prerequisite for computationally screening their redox stabilities.

These materials also have the advantage of possessing low bulk moduli (values of 8.5 GPa<sup>[18]</sup> and 22.7 GPa<sup>[17]</sup>) were calculated for LiNbOCl<sub>4</sub> at 0 K indicating that they exhibit a high compressibility. As a result, they can easily form good contact with positive electrode particles in cells with little applied pressure, and it may allow them to compensate for volume changes inside a cell on cycling. This, along with the high oxidation stabilities

of  $\text{LiMOCl}_4$ , may make them suitable for use as catholytes or coatings with high voltage cathodes. As a result, cells containing  $\text{LiNbOCl}_4$  have demonstrated capacity retention of 97% over 100 cycles at 0.3C with  $\text{LiCoO}_2$ ,<sup>[12]</sup> and 96% over 1000 cycles at 1C with  $\text{LiNi}_{0.92}\text{Co}_{0.04}\text{Mn}_{0.04}\text{O}_2$ ,<sup>[20]</sup> highlighting its effectiveness as a catholyte (Figure 6b).

In contrast, it was found that a lower capacity retention of 71.1% was reached after only 300 cycles at 1C when amorphous  $\text{LiTaOCl}_4$  was used as a catholyte with an uncoated  $\text{LiNi}_{0.9}\text{Co}_{0.05}\text{Mn}_{0.05}\text{O}_2$  (NCM955) cathode material (Figure 6c).<sup>[45]</sup> Here, the  $\text{LiTaOCl}_4$  was made amorphous as no annealing step was used. It is not immediately clear where this difference in capacity retention originates from as similar cell setups were used. However, in this case, the cycling instability of uncoated NCM955 against  $\text{LiTaOCl}_4$  was attributed to suppression of the H2-H3 phase transition in the observed  $dQ/dV^{-1}$  curves resulting in a faster capacity fade. This therefore leads to the open question whether the cation, the crystallinity, or another feature entirely also influences the differences in cycling stability of cells containing  $\text{LiNbOCl}_4$  and  $\text{LiTaOCl}_4$  catholytes. Nevertheless, by using  $\text{ZrO}_2$  coated NCM955 with the  $\text{LiTaOCl}_4$  catholyte, an improved capacity retention of 83.7% could be achieved after 500 cycles at 1C with reduced loss of the H2-H3 transition. Here, it is also worth mentioning that some halides such as  $\text{AZrCl}_6$  undergo anion exchange with  $\text{ZrO}_2$  forming interphase layers with higher ionic conductivities leading to improved capacity retention in cells.<sup>[55]</sup> Although the exact mechanism behind this behaviour has not yet been identified, it has been suggested that some halide solid electrolytes such as  $\text{Li}_3\text{InCl}_6$  can form a detrimental interphase layer with  $\text{LiNi}_{0.8}\text{Co}_{0.1}\text{Mn}_{0.1}\text{O}_2$  (NCM811) upon aging due to their poor reduction stabilities,<sup>[56]</sup> and the reduction stability of  $\text{LiTaOCl}_4$  is likely poorer still.<sup>[19]</sup>

Considering the wide electrochemical window and high cycling stabilities of cells containing  $\text{LiNbOCl}_4$ , the use of these materials as cathode coatings may also be considered. This may be further motivated by the fact that a  $\text{Li}_x\text{TaO}_x\text{F}_{5-x}$  coating was proposed to form on the surface of  $\text{LiNi}_{0.8}\text{Co}_{0.1}\text{Mn}_{0.1}\text{O}_2$  (NCM811) by heating the cathode material with 1%  $\text{TaF}_5$  at 200 °C.<sup>[57]</sup> This resulted in the in situ reaction of gaseous  $\text{TaF}_5$  with residual Li species on the surface of NCM811, such as  $\text{Li}_2\text{CO}_3$ . In doing so the authors were able to achieve an improved capacity retention of 94.0% over 500 cycles using the Li-Ta-O-F coated NCM811. Whereas, using bare NCM811, a capacity retention of just 71.8% over 100 cycles could be achieved using the same conditions.

Using  $\text{LiNbOCl}_4$  coatings (rather than Li-Ta-O-F) may also be effective in improving the cycling stability of cells. While  $\text{LiNbOCl}_4$  decomposes at temperatures above 150 °C, it may still be able to be used as a coating via mechanofusion, similar to how  $\text{Li}_3\text{InCl}_6$  has been coated onto  $\text{LiNi}_{0.8}\text{Co}_{0.15}\text{Al}_{0.05}\text{O}_2$ .<sup>[58]</sup> As such,  $\text{LiNbOCl}_4$  may also form effective cathode coatings by milling the cathode active materials with the raw reagents. The feasibility of this may also be indicated by the fact that Li-Nb-O based cathode coatings have already been shown to improve the capacity retention in solid-state batteries with NCM955<sup>[59]</sup> and  $\text{LiNi}_{0.5}\text{Mn}_{1.5}\text{O}_4$  (LMNO)<sup>[60]</sup> cathodes, and the electrochemical properties of these coatings may be further improved through halogenation.

Regardless of the cell architecture, the hazards associated with the electrochemical decomposition products of  $\text{LiMOCl}_4$  also

need to be considered in this class of material. For example, upon oxidation,  $\text{LiMOCl}_4$  is expected to form  $\text{MOCl}_3$  as well as toxic  $\text{Cl}_2$  gas.<sup>[19]</sup> Further still, the decomposition products of these materials upon heating or moisture exposure likely involves the evolution of HCl and presents additional potential hazards that need to be considered.<sup>[61]</sup> This is similar to sulphide solid electrolytes that evolve toxic  $\text{H}_2\text{S}$  upon moisture exposure, however this may be mitigated though the use of scavengers<sup>[62]</sup> or dopants.<sup>[63]</sup> Therefore, compositional and synthetic optimisation may help mitigate some of these challenges.

## 6. Composition and Optimisation

While there are several factors impeding the adoption of  $\text{LiMOCl}_4$  materials into commercial solid-state cells, adjustments in composition and synthesis methods could help overcome these issues. This includes the need to improve the reduction stability, incorporate more cost-effective elements, tune interphases, and improve the crystallinity, all while retaining (if not improving) their high ionic conductivities. In addition, exploring the structure and properties of other similar and doped materials can help elucidate the ground structure. The inherent costs associated with the  $M^{5+}$  cations (particularly  $\text{Ta}^{5+}$ ) is especially important to consider as it may limit the feasibility of commercial cells containing these materials. It also needs to be considered that both Nb and Ta are considered “critical minerals” by the United States Geological Survey (USGS) indicating that the supply chains associated with their production are vulnerable to disruption.<sup>[64]</sup>

However, due to their infancy, there has been little work done thus far on compositional modifications to  $\text{LiMOCl}_4$  materials to optimise their properties. Nevertheless, substitutions of the  $M^{5+}$  cation, or either of the two anions ( $\text{O}^{2-}$  or  $\text{Cl}^-$ ), could provide multiple degrees of freedom through which their properties may be optimised. For example, studies into the stability of  $\text{LiMOCl}_4$  ( $M = \text{Nb, Ta, Sb}$ ), and  $\text{LiMXCl}_4$  ( $M = \text{Ti, Zr, Hf, Sn}$ ;  $X = \text{Cl, F}$ ) predicted that the materials  $\text{LiZrFCl}_4$  and  $\text{LiHfFCl}_4$  have the most potential for synthesis,<sup>[19]</sup> and may hint at potential doping strategies to further improve the performance of  $\text{LiMOCl}_4$  materials. The anion stoichiometry is also important to consider as the  $\text{O}^{2-}$  content in both  $A = \text{Li}^+$  and  $\text{Na}^+$  materials correlates strongly with the crystallinity and conductivity.<sup>[16,65]</sup> Therefore, careful control of the anion ratio and anionic substitutions will be important for optimising the performance of  $\text{AMOCl}_4$  materials. In addition, aliovalent substitutions on the A site have not yet been considered which may lead to further improved conductivities by introducing additional vacancies,<sup>[66,67]</sup> or may stabilise the material by inducing greater columbic attractions connecting the chains.

Other materials with similar chemistries have also been investigated and, through these, routes toward optimising of properties of elucidating the structure of the  $\text{LiMOCl}_4$  materials may be uncovered. For example, amorphous  $\text{LiTaCl}_6$  has been reported with ionic conductivities of  $\approx 10 \text{ mS cm}^{-1}$  and can be made with varying anion stoichiometries such as  $\text{LiTaCl}_5 X_{1/n}^{n-}$ , where  $X = \text{F}^-, \text{Cl}^-, \text{Br}^-, \text{I}^-, \text{O}^{2-}, \text{OH}^-, \text{ and } \text{S}^{2-}$ .<sup>[25]</sup> However, in this case, care needs to be made to ensure their amorphous nature as crystalline  $\text{LiTaCl}_6$  has conductivities of  $\approx 10^{-5} \text{ mS cm}^{-1}$ .<sup>[68]</sup>

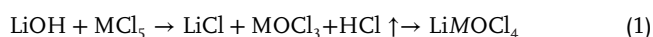
Other A–M–O–Cl solid electrolytes have also been studied. For example,  $\text{AAO}_x\text{Cl}_{4-2x}$  ( $A = \text{Li}^+$  or  $\text{Na}^+$ ) materials have also been synthesised with polymer-like viscoelasticity and ionic conductivities of up to  $1.52 \text{ mS}\cdot\text{cm}^{-1}$  allowing for improved contact with electrode materials.<sup>[53,69]</sup> In addition, the amorphous  $x\text{Li}_2\text{O}\text{-HfCl}_4$  materials have been synthesised, with the composition  $\text{Li}_2\text{HfOCl}_4$  ( $x = 1$ ) demonstrating an ionic conductivity of  $0.93 \text{ mS}\cdot\text{cm}^{-1}$ <sup>[70]</sup> and, similarly, amorphous  $\text{Li}_2\text{La}_{0.5}\text{Ta}_{0.5}\text{OCl}_4$  has been produced mechanochemically<sup>[71]</sup> hinting at the possibility of stable  $\text{La}^{3+}$  or  $\text{Hf}^{4+}$  for  $M^{5+}$  substitutions in  $\text{LiMOCl}_4$ . As such, the investigation of solid solutions between  $\text{LiMOCl}_4$  and these other similar materials may lead to further improved ionic conductivities.

Notably, while there are many degrees of freedom with which the  $\text{LiMOCl}_4$  materials may be optimised, the potential strategies listed above do not reflect a rational or targeted approach toward desired properties. This need again highlights the importance of a combined experimental and theoretical approach as it is not possible to rationally target desired properties if the mechanisms behind those properties are unknown. For example, as mentioned earlier, introducing  $M$ -cation substitutions that influence the  $[\text{MOCl}_4]_{\infty}^-$  chain rigidity could help to establish the extent to which this structural feature benefits or hinders the ionic conductivity, and could help to uncover the underlying crystal structure. From this point, it would then be possible to work backward and target compositions or structures with designed chain rigidities specifically to maximise the ionic conductivity. However, again, this is not possible with representative atomistic structures being unknown.

While compositional optimisation is needed to improve the electrochemical properties, new synthesis routes are needed to make  $\text{LiMOCl}_4$  materials at scale and with high crystallinities. Not only is this important for understanding the structure-property relationships in these materials, but it has been also shown that the ionic conductivities are proportional to the coherence lengths in these materials.<sup>[16,17]</sup> Therefore, synthetic (as well as compositional) optimisations can also provide routes toward improved electrochemical performances in  $\text{LiMOCl}_4$ .

## 7. Synthesis and Processing

To see their adoption into commercial solid-state cells, both the synthesis and processing techniques for producing  $\text{LiMOCl}_4$  materials also need to be optimised. Thus far, two mechanochemical synthesis routes toward  $\text{LiMOCl}_4$  ( $M = \text{Nb}^{5+}$ ,  $\text{Ta}^{5+}$ ) have been identified. These materials were first synthesised by milling  $\text{LiOH}$  and  $\text{MCl}_5$  together at high energies for 40 hs before annealing them at 100 and 300 °C for  $\text{LiNbOCl}_4$  and  $\text{LiTaOCl}_4$ , respectively, all under inert conditions. In this reaction,  $\text{LiCl}$  and  $\text{MOCl}_3$  are produced as intermediates with gaseous  $\text{HCl}$  as a by-product (Reaction 1).<sup>[20]</sup>  $\text{LiNbOCl}_4$  has been also shown to be synthesisable directly from the  $\text{LiCl}$  and  $\text{NbOCl}_3$  intermediates (Reaction 2), avoiding the formation of corrosive  $\text{HCl}$ .<sup>[20]</sup>



The  $\text{LiMOCl}_4$  materials possess the advantage that their synthesis is simple and scalable, and it has been further shown that milling times can be shortened to just 4 h whilst still achieving a high ionic conductivity of  $5.03 \text{ mS}\cdot\text{cm}^{-1}$  in  $\text{LiTaOCl}_4$ .<sup>[45]</sup> Although the  $\text{LiMCl}_6$  materials have ionic conductivities that approach that of  $\text{LiMOCl}_4$  when amorphous, actually making these materials amorphous requires milling times exceeding 140 h<sup>[25]</sup> and has limited reproducibility.<sup>[21]</sup> As such, the mechanochemical route to produce  $\text{LiMOCl}_4$  can therefore be advantageous due to the rapid synthesis times. Despite this, the evolution of the corrosive and gaseous  $\text{HCl}$  byproduct when  $\text{LiOH}$  and  $\text{MCl}_5$  are used needs to be dealt with appropriately to ensure safety and the pressure limits of synthesis containers are not exceeded. In addition, upon their synthesis, the absence of  $\text{HCl}$  / proton contamination in  $\text{LiMOCl}_4$  would need to be verified by  $^1\text{H}$  NMR to confirm that there is no loss of active species that are being replaced by  $\text{H}^+$ , and to prevent any potential damage to the other cell components. Even if  $\text{LiCl}$  and  $\text{MOCl}_3$  were used as starting reagents, the use of  $\text{MOCl}_3$  may incur additional expenses associated with its synthesis or purchase that would need to be considered.

These materials may also be synthesised using other  $\text{O}^{2-}$  sources avoiding the formation of  $\text{HCl}$ , similar to some other  $\text{Li-M-O-Cl}$  glasses. For example, an amorphous  $x\text{Li}_2\text{O-TaCl}_5$  series ( $1 \leq x \leq 2$ ),<sup>[70]</sup> as well as  $\text{LiTaCl}_5\text{O}_{0.5}$ ,<sup>[25]</sup> can be synthesised mechanochemically from  $\text{Li}_2\text{O}$  and  $\text{Li}_2\text{O}_2$ , respectively (although these also incur their own respective cost and hazard risks). The  $\text{LiTaOCl}_4$  composition has also been reported to be synthesised by milling  $\text{LiTaO}_3$ ,  $\text{TaCl}_5$  and  $\text{LiCl}$  together.<sup>[72]</sup> In this case, only peaks form a poorly crystalline  $\text{LiTaO}_3$ -like phase are observed in the diffraction patterns. Here, the authors achieve an ionic conductivity of  $\sim 8 \text{ mS}\cdot\text{cm}^{-1}$  for their  $\text{LiTaOCl}_4$  and suggest this is due to the substitution of  $\text{Cl}^-$  for  $\text{O}^{2-}$  in  $\text{LiTaO}_3$ . However, as no annealing step was performed, it is feasible that the  $\text{LiTaOCl}_4$  was simply fully amorphous the  $\text{LiTaO}_3$ -like product is simply unreacted starting material. While this is another potential route toward  $\text{LiMOCl}_4$  avoiding the formation of  $\text{HCl}$ , more research needs to be performed to study the structure and composition of  $\text{LiMOCl}_4$  materials synthesised using this method.

Regardless of these processing complexities, due to the softness of these materials, the mechanochemical synthesis procedure also results in powder products that have poor crystallinities making them difficult to study with diffraction-based techniques. As such, the depth of structural information one can obtain is inherently limited by using the current mechanochemical synthesis routes. In addition, as the ionic conductivities of  $\text{LiMOCl}_4$  are proportional to their coherence lengths,<sup>[16]</sup> it will also hamper their performance in cells. Finally, it may also limit one's ability to tune the particle size distribution, which is important to consider as differences in microstructure and void space between particles in the cathode composite can impede charge carrier transport resulting in lower obtainable capacities in cells.<sup>[73]</sup> This again highlights the need for a combined experimental-theoretical approach where the synthesis of metastable materials may be realised, e.g., through the kinetic control of a reaction.<sup>[74]</sup> Clearly, alternative synthesis routes toward  $\text{LiMOCl}_4$  materials are needed to mitigate the complexities and safety concerns originating from the  $\text{HCl}$  by-product. For example, a deeper understanding of their stability in air and solvents would potentially allow for their synthesis and processing using alternate routes,

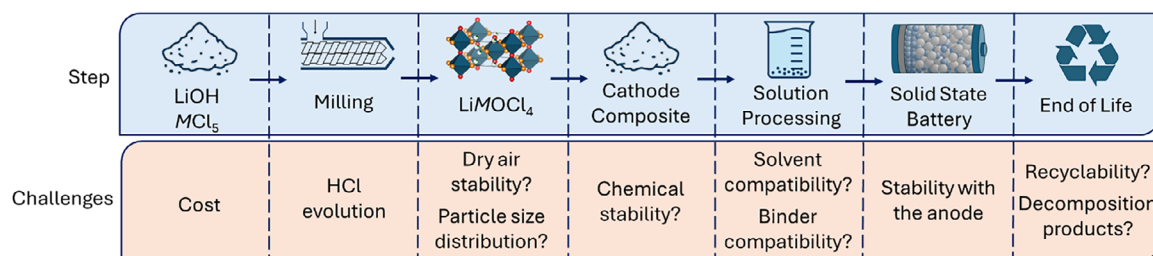


**Figure 7.** The steps required to take LiOH and MCl<sub>5</sub> make them into an all-solid-state-battery containing LiMOCl<sub>4</sub> and highlighting the challenges and unknowns (indicated with “?”) associated with each step.

or in dry rooms using high throughput mechanochemical synthesis apparatus,<sup>[75–77]</sup> rather than in purely inert atmospheres.

More research is also needed to understand how these materials may be processed into cells after synthesis. The processing of powders into solid-state batteries can additionally be challenging as appropriate binder-solvent combinations are often required to make high quality films, and the solid electrolyte must be compatible with both.<sup>[78]</sup> Currently, solid electrolytes can be processed into all-solid-state-batteries using solvents in one of two ways. Either through slurry casting<sup>[79,80]</sup> where the solid electrolyte material is not dissolved, or through an infiltration / coating process<sup>[81,82]</sup> where the electrolyte is dissolved. Either way, the compatibility of LiMOCl<sub>4</sub> with different solvents and binders needs to be assessed. However, it is unlikely that the LiMOCl<sub>4</sub> materials will be able to be recrystallised from (or be stable in) protic solvents, as the presence of structural H<sup>+</sup> is already a concern.

A viable alternative to producing LiMOCl<sub>4</sub> films with solvents is via a dry-film process – although this is less well established.<sup>[83]</sup> This has the added advantages of reduced costs, waste, and use of poisonous solvents. However, it also comes with its own added complexities as making homogenous mixtures of dry powders is inherently harder without the use of a liquid medium.<sup>[84]</sup> In addition, carefully tuned particle sizes are also needed for dry-film fabrication and the particle size distributions of the LiMOCl<sub>4</sub> materials are difficult to control, and the optimal particle sizes for film production may not be optimal for cell performance. Nevertheless, the low annealing temperature of 100 °C for LiNbOCl<sub>4</sub><sup>[12]</sup> may allow for cathode composites to be hot pressed resulting in improved contact between grains and improved crystallinity while avoiding any decomposition reactions between it and the active material.<sup>[85,86]</sup>

How these materials are processed at end-of-life should be considered before they can be effectively implemented into solid-state batteries. This includes, as mentioned earlier, considering their decomposition products, but also how they may be recycled or reclaimed from used solid-state batteries.<sup>[87]</sup> A summary of the challenges that need to be addressed in the synthesis and processing optimisations of LiMOCl<sub>4</sub> is given in **Figure 7**.

Further, as discussed earlier, the poor reduction stability of these materials would also result in an increased cost of manufacturing cells containing LiMOCl<sub>4</sub> separators, as they would likely have to contain an interfacial layer with the anode that would incur additional costs and reduce volumetric and gravimetric capacities.<sup>[52]</sup> As such, the cost of Nb<sup>5+</sup> and Ta<sup>5+</sup> may decrease the economic viability of LiMOCl<sub>4</sub> materials as either

catholytes or as separator layers. Nevertheless, any issues related to cost may be significantly mitigated if LiMOCl<sub>4</sub> materials can be used as cathode active material coatings instead, as only very small amounts of material are needed—typically ≈1 wt.% of the mass of the active material.<sup>[57,88]</sup>

## 8. Comparing Lithium and Sodium in NaMOCl<sub>4</sub> and LiMOCl<sub>4</sub>

Much of the research on AMOCl<sub>4</sub> has focused on Li-containing materials, however both A = Na<sup>+</sup> materials (NaNbOCl<sub>4</sub> and NaTaOCl<sub>4</sub>) have also been synthesised<sup>[13,14,65]</sup> and exhibit several key similarities and differences. Starting with their synthesis, both the A = Na<sup>+</sup> materials have been produced mechanochemically starting with NaOH and MCl<sub>5</sub>,<sup>[13,14]</sup> and NaNbOCl<sub>4</sub> also with NaCl and MOCl<sub>3</sub>.<sup>[65]</sup> As such, these materials also have the advantage of an efficient and scalable synthesis procedure, and without the formation of HCl if it is required. To achieve a HCl-free synthesis, other oxygen sources may also be employed, such as Na<sub>2</sub>O<sub>2</sub> and Na<sub>2</sub>O, which has been used to produce xNa<sub>2</sub>O<sub>2</sub>-TaCl<sub>5</sub><sup>[89]</sup> and xNa<sub>2</sub>O-TaCl<sub>5</sub><sup>[30]</sup> glasses, respectively.

When synthesised using NaOH and MCl<sub>5</sub>, both NaMOCl<sub>4</sub> materials show no, or extremely broad, reflections in their diffraction patterns<sup>[13,14]</sup> indicating that they have even shorter coherence lengths or more disordered chains than in the A = Li<sup>+</sup> analogues (**Figure 8a**), and again the M = Nb<sup>5+</sup> compounds generally show slightly higher crystallinities than those with M = Ta<sup>5+</sup>. In contrast, when synthesised using NaCl and NbOCl<sub>3</sub>, NaNbOCl<sub>4</sub> samples showed improved crystallinities allowing them to be studied via powder diffraction.<sup>[65]</sup> Through which, it was suggested that the NaNbOCl<sub>4</sub> also exhibits the I4/m long-range structure – although detailed structural refinements have not yet been performed.

Due to different techniques being used to study different AMOCl<sub>4</sub> materials that are made also using different procedures, it is currently difficult to directly compare the structures of the A = Li<sup>+</sup> and Na<sup>+</sup> materials. As such, **Figure 7** compares the X-ray diffraction patterns of LiTaOCl<sub>4</sub><sup>[12]</sup> and NaTaOCl<sub>4</sub>,<sup>[13]</sup> and the X-ray pair distribution functions of LiNbOCl<sub>4</sub><sup>[17]</sup> and NaTaOCl<sub>4</sub><sup>[13]</sup> – all of which were synthesised using AOH and MCl<sub>5</sub>. However, it should be noted here that these samples were also prepared using different annealing temperatures; 300 °C for the LiTaOCl<sub>4</sub> sample studied by X-ray diffraction, and 100 °C for the remainder. Nevertheless, this data is presented to show that NaMOCl<sub>4</sub> is expected to retain the 1D [MOCl<sub>4</sub>]<sub>∞</sub><sup>-</sup> chains that are surrounded by various A<sup>+</sup> cation sites, as was observed in LiNbOCl<sub>4</sub>.<sup>[13,14]</sup>

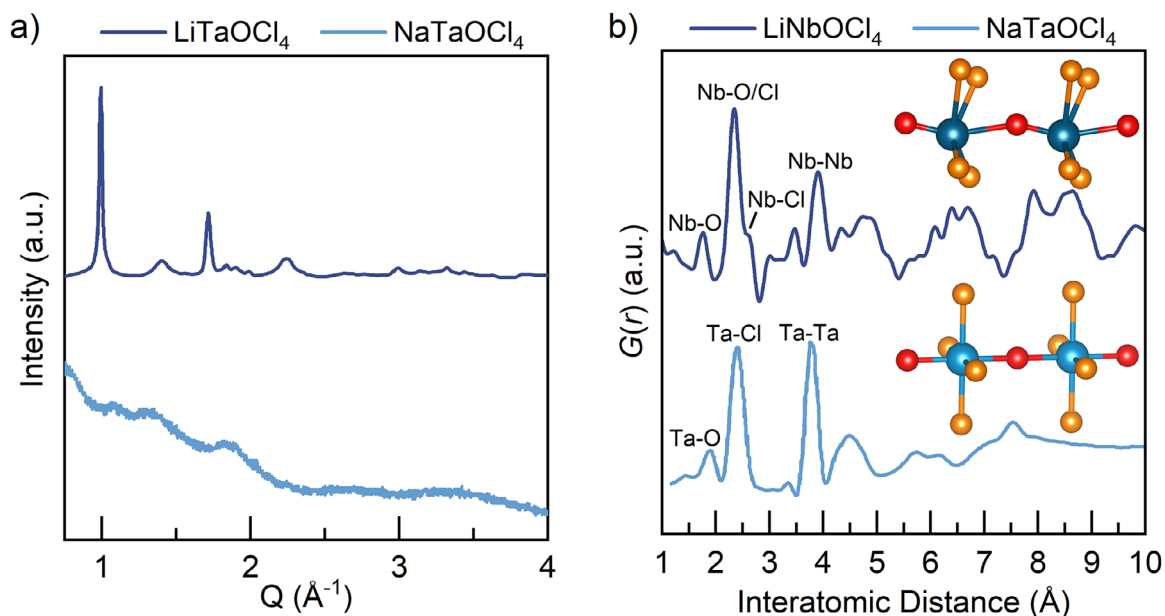


**Figure 8.** A comparison of the a) X-ray diffraction patterns of  $\text{LiTaOCl}_4$ <sup>[12]</sup> and  $\text{NaTaOCl}_4$ <sup>[13]</sup> and b) X-ray PDF of  $\text{LiNbOCl}_4$ <sup>[17]</sup> and  $\text{NaTaOCl}_4$ <sup>[13]</sup> The inserts show the structures of the  $\text{MO}_2\text{Cl}_4$  polyhedra that can be inferred from the PDF data. Data digitised from refs.[12, 13, 17]

However, in contrast to  $\text{LiNbOCl}_4$ , there is no clear indication of two different  $M\text{-O}$  bond lengths in  $\text{NaTaOCl}_4$  indicating that it might retain a higher symmetry local structure (Figure 8b). However, without neutron PDF on the  $A = \text{Na}^+$  materials to detect the light  $\text{O}^{2-}$  relative to  $\text{Nb}^{5+}$  or  $\text{Ta}^{5+}$ , this is difficult to say with confidence. As such, no definitive local or long-range structural model has yet been proposed for either of the  $\text{NaMOCl}_4$  materials. Therefore, many of the challenges in understanding the structure-property relationships in the  $\text{Li}^+$  materials are amplified for  $\text{Na}^+$ , and it becomes harder still to make informed choices into how certain dopants may benefit or hinder the properties of the  $\text{NaMOCl}_4$  materials.

The ionic conductivities of the of  $\text{NaNbOCl}_4$  and  $\text{NaTaOCl}_4$  are about an order of magnitude lower than the  $A = \text{Li}^+$  materials at 1.2 and 1.5  $\text{mS}\cdot\text{cm}^{-1}$ , respectively.<sup>[14]</sup> As such, their optimisation remains a priority. It should also be noted that  $\text{NaTaCl}_6$  has reported ionic conductivities of 4  $\text{mS}\cdot\text{cm}^{-1}$  when made amorphous.<sup>[90]</sup> As this has an ionic conductivity higher than that of  $\text{NaTaOCl}_4$ , the incorporation of  $\text{O}^{2-}$  needs to be better justified if it does not significantly improve the ionic conductivity relative to the pure amorphous halide.

Nevertheless, while the  $\text{NaMOCl}_4$  materials have not yet been optimised for their ionic conductivities, similar materials have been substituted, providing several potential routes toward further improved properties. For example, it has been shown that it is possible to achieve a solid solution across the entire range of  $\text{Na}_{1+x}\text{M}_{1-x}\text{Zr}_x\text{Cl}_6$  ( $M = \text{Nb}^{5+}, \text{Ta}^{5+}$ ), with the ionic conductivity being maximised when  $x \approx 0.5$  in each.<sup>[91]</sup> As such, this may indicate that  $\text{Zr}^{4+}$  for  $M^{5+}$  substitutions in  $\text{NaMOCl}_4$  may be energetically favourable and may lead to further improved ionic conductivities.

Similar redox stabilities have also been observed for the  $A = \text{Li}^+$  and  $\text{Na}^+$  materials. For example,  $\text{NaTaOCl}_4$  has reduction and oxidation potentials of 2.5 and 4.0 V respectively versus  $\text{Na}^+/\text{Na}$ .<sup>[13]</sup>

As such, the  $\text{NaMOCl}_4$  solid electrolytes are also unstable against  $\text{Na}$  metal anodes, resulting in them requiring the use of an additional separator layer if they are to be used as catholytes or separators.<sup>[14]</sup> Nevertheless, when using  $\text{NaTaOCl}_4$  as a catholyte with a  $\text{Na}_{2/3}\text{Ni}_{1/3}\text{Mn}_{2/3}\text{O}_2$  cathode active material, a capacity retention of 89.5% could be obtained over 250 cycles at 1/3C.<sup>[13]</sup>

These findings show that both the  $A = \text{Li}^+$  and  $\text{Na}^+$  face similar challenges in their optimisation for adoption in commercial solid-state batteries. Despite this, the extremely poor crystallinity of the  $\text{NaMOCl}_4$  materials will likely make understanding the chemistry behind these challenges harder still. However, they do still possess high mobilities and an efficient and scalable synthesis procedure that advantages them for use in post Li-ion batteries. While only the  $A = \text{Li}^+$  and  $\text{Na}^+$  materials have been discussed in depth here, the existence of materials with similar chemistries but with different mobile ions, such as  $\text{KMCl}_6$  ( $M = \text{Nb}$  and  $\text{Ta}$ ), hints that the broad compositional flexibility that may be offered by the  $\text{AMOCl}_4$  class of materials for other applications.<sup>[92,93]</sup>

## 9. Outlook and Key Challenges

The  $\text{AMOCl}_4$  class of materials present many attractive properties for use as  $\text{Li}^+$  and  $\text{Na}^+$  ion conductors. This is primarily due to their high ionic conductivities which are enabled by the correlated motion, flexible 1D chains, and unimpeded conduction pathways. In addition, their high oxidation stability makes them usable as catholytes with high voltage cathode active materials, and their simple and fast synthesis routes make these materials suitable for industrial scale up. As such, these materials are an attractive option for use as catholyte or cathode coatings in all solid-state batteries. Despite these benefits, several key challenges and unknowns remain.

Many of the challenges that surround the  $\text{AMOC}_4$  materials can be traced back to the required mechanochemical synthesis procedure. Not only because the formation of a HCl by-product risks exceeding the pressure limits of containers (although this can be mitigated by using  $\text{MOCl}_3$ ), but also because it results in the formation of a glass-ceramic product with extremely short coherence lengths. This in turn means that a full structural solution cannot be developed, structure-property relationships cannot be inferred, and theoretical models that rely on long range ordering cannot be used. As a result, this also restricts our ability to make informed optimisation strategies or to design other materials with further improved properties for use in solid-state batteries.

In addition to synthesis, structure, and property related challenges, there are several unknowns related to the processing and handling requirements of the  $\text{AMOC}_4$  materials that need to be addressed. First, their chemical stability against different cathode active materials and coatings needs to be fully assessed. In addition, their poor reduction stabilities require the use of an additional separator layer that is stable against the anode resulting in higher costs and thickness in cells if they are used as catholytes. It is further currently unknown, which solvents and binders are most compatible with  $\text{AMOC}_4$  materials, nor how their particle sizes can be tuned, all of which are essential for the industrial scale production of solid-state batteries.

Future research into these challenges will help to mitigate their detrimental effects. Here, we emphasise the requirement of a two pronged experimental and theoretical approach when tackling the challenges surrounding the  $\text{AMOC}_4$  materials. For example, studying reaction kinetics and thermodynamics in attempts to synthesise  $\text{AMOC}_4$  with longer coherence lengths, using diffraction and spectroscopic techniques alongside structure relaxations to uncover the structural ground states, as well as studying dopant effects and simulations to elucidate the structure-property relationships. In all, this oxyhalide class of ionic conductors appears more challenging to understand than previous fast ionic conductors. However, the currently existing data suggests that, once these prior research challenges have been addressed, the  $\text{LiMOCl}_4$  and  $\text{NaMOCl}_4$  materials represent promising candidates for adoption into all-solid-state-batteries.

## Acknowledgements

The authors thank the Bundesministerium für Forschung, Technologie und Raumfahrt (BMFTR) for funding under the FESTBATT cluster of competence (project 03XP0430F). J.A. Newnham wishes to acknowledge Dr. H. Slocombe for the fruitful discussions that lead to the completion of this perspective.

Open access funding enabled and organized by Projekt DEAL.

## Conflict of Interest

The authors declare no conflict of interest.

## Keywords

oxyhalides, Solid electrolytes, Solid state batteries

Received: July 22, 2025  
Revised: August 19, 2025  
Published online: September 12, 2025

- [1] J. Mitali, S. Dhinakaran, A. A. Mohamad, *Energy Storage Sav.* **2022**, *1*, 166.
- [2] J. B. Goodenough, K.-S. Park, *J. Am. Chem. Soc.* **2013**, *135*, 1167.
- [3] C. Wang, C. Yang, Z. Zheng, *Adv. Sci.* **2022**, *9*, 2105213.
- [4] J. Janek, W. G. Zeier, *Nat. Energy* **2023**, *8*, 230.
- [5] S. Wang, Q. Bai, A. M. Nolan, Y. Liu, S. Gong, Q. Sun, Y. Mo, *Angew. Chem., Int. Ed.* **2019**, *58*, 8039.
- [6] J. Park, J. P. Son, W. Ko, J.-S. Kim, Y. Choi, H. Kim, H. Kwak, D.-H. Seo, J. Kim, Y. S. Jung, *ACS Energy Lett.* **2022**, *7*, 3293.
- [7] H. Kwak, D. Han, J. Lyoo, J. Park, S. Hoo Jung, Y. Han, G. Kwon, H. Kim, S.-T. Hong, K.-W. S. Nam, Y. Jung, H. Kwak, J. Park, S. H. Jung, Y. Han, Y. S. Jung, H. Kim, D. Han, K. Nam, J. Lyoo, S. Hong, G. Kwon, *Adv. Energy Mater.* **2021**, *11*, 2003190.
- [8] X. Li, J. Liang, N. Chen, J. Luo, K. R. Adair, C. Wang, M. N. Banis, T.-K. Sham, L. Zhang, S. Zhao, S. Lu, H. Huang, R. Li, X. Sun, *Angew. Chem.* **2019**, *131*, 16579.
- [9] A. Manthiram, X. Yu, S. Wang, *Nat. Rev. Mater.* **2017**, *2*, 16103.
- [10] J. D. Luo, Y. Zhang, X. Cheng, F. Li, H. Y. Tan, M. Y. Zhou, Z. W. Wang, X. D. Hao, Y. C. Yin, B. Jiang, H. B. Yao, *Angew. Chem., Int. Ed.* **2024**, *63*, 202400424.
- [11] K. Barker, S. L. McKinney, R. Artal, R. Jiménez, N. Tapia-Ruiz, S. J. Skinner, A. Aguadero, I. D. Seymour, *Nat. Commun.* **2024**, *15*, 7501.
- [12] Y. Tanaka, K. Ueno, K. Mizuno, K. Takeuchi, T. Asano, A. Sakai, Y. Tanaka, K. Ueno, K. Mizuno, K. Takeuchi, T. Asano, A. Sakai, *Angew. Chem.* **2023**, *135*, 202217581.
- [13] L. Zhou, J. D. Bazak, C. Li, L. F. Nazar, *ACS Energy Lett.* **2024**, *9*, 4093.
- [14] T. Zhao, B. Samanta, X. M. de Irujo-Labelde, G. Whang, N. Yadav, M. A. Kraft, P. Adelhelm, M. R. Hansen, W. G. Zeier, *ACS Mater. Lett.* **2024**, *6*, 3683.
- [15] S. Ferrari, M. Falco, A. B. Muñoz-García, M. Bonomo, S. Brutti, M. Pavone, C. Gerbaldi, *Advanced Energy Materials*, John Wiley and Sons Inc, Hoboken, New Jersey **2021**.
- [16] J. A. Newnham, J. Kondek, J. Hartel, C. Rosenbach, C. Li, V. Faka, L. Gronych, D. Glikman, F. Schreiner, D. D. Wind, B. Braunschweig, M. R. Hansen, W. G. Zeier, *Chem. Mater.* **2025**, *37*, 4130.
- [17] B. Singh, Y. Wang, J. Liu, J. D. Bazak, A. Shyamsunder, L. F. Nazar, *J. Am. Chem. Soc.* **2024**, *146*, 17158.
- [18] S. Adams, *Energy Storage Mater.* **2024**, *68*, 103359.
- [19] K. J. Jun, G. Wei, X. Yang, Y. Chen, G. Ceder, *Matter* **2025**, *8*, 102001.
- [20] S. Jeon, K. H. Park, W. Cho, G. Jeong, J. Yu, Y. J. Park, K. S. Kim, *Solid State Ionics* **2025**, *421*, 116791.
- [21] A. Chaupatnaik, G. Rousse, A. J. Perez, A. V. Morozov, E. Elkaim, M. Avdeev, A. M. Abakumov, J. Tarascon, *Adv. Energy Mater.* **2024**, *14*, 2402555.
- [22] J. Beck, J. Bordinhão, *Z. Anorg. Allg. Chem.* **2005**, *631*, 1261.
- [23] M. Ströbele, H.-J. Meyer, *Z. Anorg. Allg. Chem.* **2002**, *628*, 488.
- [24] M. J. Fallon, V. Faka, M. A. Lange, M. A. Kraft, E. Suard, E. T. Connolly, B. E. Francisco, A. G. Squires, W. G. Zeier, *J. Am. Chem. Soc.* **2025**, *147*, 10151.
- [25] Y. Ishiguro, K. Ueno, S. Nishimura, G. Iida, Y. Igarashib, *Chem. Lett.* **2023**, *52*, 237.
- [26] X. Martinez de Irujo-Labelde, T. Zhao, B. Samanta, T. Bernges, V. Faka, A. N. Sobolev, O. Maus, M. Appel, M. A. Kraft, M. R. Hansen, W. G. Zeier, *J. Mater. Chem. A* **2024**, *12*, 33707.
- [27] H. Henke, *Z. Kristallogr. Cryst. Mater.* **1992**, *198*, 1.
- [28] O. Zakary, M. Body, V. Sarou-Kanian, B. Arnaud, G. Corbel, C. Legein, *J. Alloys Compd.* **2025**, *1010*, 177457.

- [29] C.-W. Lee, M. Maegawa, H. Akamatsu, K. Hayashi, S. Ohno, P. Gorai, *ACS Mater. Lett.* **2025**, 7, 620.
- [30] Z. Huang, N. Yadav, P. Song, H. Akamatsu, K. Hayashi, P. Gorai, S. Ohno, *Energy* **2025**.
- [31] E. B. Jones, V. Stevanović, *npj Comput. Mater.* **2020**, 6, 56.
- [32] L. Wolf, A. Novick, V. Stevanović, *J. Appl. Phys.* **2025**, 137, 95101.
- [33] G. Krenzer, C. E. Kim, K. Tolborg, B. J. Morgan, A. Walsh, *J. Mater. Chem. A* **2022**, 10, 2295.
- [34] Y. Li, Z. Deng, C. Chen, P. Canepa, *Chem. Mater.* **2024**, 36, 7877.
- [35] B. J. Morgan, *Chem. Mater.* **2021**, 33, 2004.
- [36] J. G. Smith, D. J. Siegel, *Nat. Commun.* **2020**, 11, 1483.
- [37] M. Sadowski, K. Albe, *J. Power Sources* **2020**, 478, 229041.
- [38] A. R. Symington, J. Purton, J. Statham, M. Molinari, M. S. Islam, S. C. Parker, *J. Mater. Chem. A* **2020**, 8, 19603.
- [39] F. N. Forrester, J. A. Quirk, T. Famprakis, J. A. Dawson, *Chem. Mater.* **2022**, 34, 10561.
- [40] X. Li, J. Liang, J. Luo, M. Norouzi Banis, C. Wang, W. Li, S. Deng, C. Yu, F. Zhao, Y. Hu, T. K. Sham, L. Zhang, S. Zhao, S. Lu, H. Huang, R. Li, K. R. Adair, X. Sun, *Energy Environ. Sci.* **2019**, 12, 2665.
- [41] X. Luo, Y. Zhong, X. Wang, X. Xia, C. Gu, J. Tu, *ACS Appl. Mater. Interfaces* **2022**, 14, 49839.
- [42] X. Li, J. Liang, N. Chen, J. Luo, K. R. Adair, C. Wang, M. N. Banis, T. Sham, L. Zhang, S. Zhao, S. Lu, H. Huang, R. Li, X. Sun, *Angew. Chem.* **2019**, 131, 16579.
- [43] B. Helm, R. Schlem, B. Wankmiller, A. Banik, A. Gautam, J. Ruhl, C. Li, M. R. Hansen, W. G. Zeier, *Chem. Mater.* **2021**, 33, 4773.
- [44] S. Hori, R. Kanno, O. Kwon, Y. Kato, T. Yamada, M. Matsuura, M. Yonemura, T. Kamiyama, K. Shibata, Y. Kawakita, *J. Phys. Chem. C* **2022**, 126, 9518.
- [45] L. Li, Z. Jiang, J. Yang, C. Liu, Q. Luo, S. Li, L. Zhang, X. Chen, S. Cheng, C. Yu, *Adv. Funct. Mater.* **2024**, 35, 2410008.
- [46] K. Kim, D. Park, H.-G. Jung, K. Y. Chung, J. H. Shim, B. C. Wood, S. Yu, *Chem. Mater.* **2021**, 33, 3669.
- [47] Y. Zhu, X. He, Y. Mo, *ACS Appl. Mater. Interfaces* **2015**, 7, 23685.
- [48] F. Han, Y. Zhu, X. He, Y. Mo, C. Wang, *Adv. Energy Mater.* **2016**, 6, 1501590.
- [49] T. Krauskopf, F. H. Richter, W. G. Zeier, J. Janek, *Chem. Rev.* **2020**, 120, 7745.
- [50] G. F. Dewald, S. Ohno, M. A. Kraft, R. Koerver, P. Till, N. M. Vargas-Barbosa, J. Janek, W. G. Zeier, *Chem. Mater.* **2019**, 31, 8328.
- [51] C. D. Alt, N. U. C. B. Müller, L. M. Riegger, B. Aktekin, P. Minnmann, K. Peppler, J. Janek, *Joule* **2024**, 8, 2755.
- [52] C. Rosenbach, F. Walthert, J. Ruhl, M. Hartmann, T. A. Hendriks, S. Ohno, J. Janek, W. G. Zeier, *Adv. Energy Mater.* **2023**, 13, 2203673.
- [53] T. Dai, S. Wu, Y. Lu, Y. Yang, Y. Liu, C. Chang, X. Rong, R. Xiao, J. Zhao, Y. Liu, W. Wang, L. Chen, Y.-S. Hu, *Nat. Energy* **2023**, 8, 1221.
- [54] L. M. Riegger, R. Schlem, J. Sann, W. G. Zeier, J. Janek, *Angew. Chem., Int. Ed.* **2021**, 60, 6718.
- [55] H. Kwak, J. S. Kim, D. Han, J. S. Kim, J. Park, G. Kwon, S. M. Bak, U. Heo, C. Park, H. W. Lee, K. W. Nam, D. H. Seo, Y. S. Jung, *Nat. Commun.* **2023**, 14, 2459.
- [56] W. Kim, J. Noh, S. Lee, K. Yoon, S. Han, S. Yu, K. Ko, K. Kang, *Adv. Mater.* **2023**, 35, 2301631.
- [57] Y. Liu, T. Yu, S. Xu, Y. Sun, J. Li, X. Xu, H. Li, M. Zhang, J. Tian, R. Hou, Y. Rao, H. Zhou, S. Guo, *Angew. Chem., Int. Ed.* **2024**, 63, 202403617.
- [58] F. Jin, L. Fadillah, H. Q. Nguyen, T. M. Sandvik, Y. Liu, A. Garcia-Martín, E. Salagre, E. G. Michel, D. Stoian, K. Marshall, W. Van Beek, G. Redhammer, M. Mehraj Ud Din, D. Rettenwander, *Chem. Mater.* **2024**, 36, 6017.
- [59] F. Xin, A. Goel, X. Chen, H. Zhou, J. Bai, S. Liu, F. Wang, G. Zhou, M. S. Whittingham, *Chem. Mater.* **2022**, 34, 7858.
- [60] G. Gabrielli, P. Axmann, T. Diemant, R. J. Behm, M. Wohlfahrt-Mehrens, *ChemSusChem* **2016**, 9, 1670.
- [61] T. Usami, N. Tanibata, H. Takeda, M. Nakayama, *J. Solid State Electrochem.* **2024**, 28, 4427.
- [62] D. Lee, K. H. Park, S. Y. Kim, J. Y. Jung, W. Lee, K. Kim, G. Jeong, J. S. Yu, J. Choi, M. S. Park, W. Cho, *J. Mater. Chem. A* **2021**, 9, 17311.
- [63] T. Ohtomo, A. Hayashi, M. Tatsumisago, K. Kawamoto, *J. Mater. Sci.* **2013**, 48, 4137.
- [64] U.S. Geological Survey., *Mineral Commodity Summaries* **2025**.
- [65] S. Kmiec, E. Ruoff, A. Manthiram, *Angew. Chem., Int. Ed.* **2025**, 64, 202416979.
- [66] P. Adeli, J. D. Bazak, A. Huq, G. R. Goward, L. F. Nazar, *Chem. Mater.* **2021**, 33, 146.
- [67] L. Buannic, B. Orayech, J.-M. López Del Amo, J. Carrasco, N. A. Katcho, F. Aguesse, W. Manalastas, W. Zhang, J. Kilner, A. Llordés, *Chem. Mater.* **2017**, 29, 1769.
- [68] A. Chaupatnaik, G. Rouse, A. J. Perez, A. V. Morozov, E. Elkaïm, M. Avdeev, A. M. Abakumov, J. M. Tarascon, *Adv. Energy Mater.* **2024**, 14, 2402555.
- [69] I. You, B. Singh, M. Cui, G. Goward, L. Qian, Z. Arthur, G. King, L. F. Nazar, *Energy Environ. Sci.* **2025**, 18, 478.
- [70] S. Zhang, F. Zhao, J. Chen, J. Fu, J. Luo, S. H. Alahakoon, L.-Y. Chang, R. Feng, M. Shakouri, J. Liang, Y. Zhao, X. Li, L. He, Y. Huang, T.-K. Sham, X. Sun, *Nat. Commun.* **2023**, 14, 3780.
- [71] S. Song, F. Wei, W. Xue, Y. Cui, Z. Long, H. Shan, N. Hu, *J. Mater. Chem. A* **2025**, 13, 26478.
- [72] W. Xue, Y. Cui, Z. Long, H. Shan, N. Chamidah, K. Yamamoto, M. Kotobuki, H. Li, N. Hu, S. Song, *J. Phys. Chem. Lett.* **2025**, 16, 8283.
- [73] E. Schlautmann, A. Weiß, O. Maus, L. Ketter, M. Rana, S. Puls, V. Nickel, C. Gabbey, C. Hartnig, A. Bielefeld, W. G. Zeier, *Adv. Energy Mater.* **2023**, 13, 2302309.
- [74] J. R. Chamorro, T. M. McQueen, *Acc. Chem. Res.* **2018**, 51, 2918.
- [75] D. E. Crawford, C. K. G. Miskimmin, A. B. Albadarin, G. Walker, S. L. James, *Green Chem.* **2017**, 19, 1507.
- [76] M. Grube, M. Hofer, M. Witt, J. Schubert, J. Janek, W. G. Zeier, A. Kwade, S. Zellmer, *J. Energy Storage* **2025**, 121, 116593.
- [77] G. Kaupp, J. Schmeyers, M. R. Naimi-Jamal, H. Zoz, H. Ren, *Chem. Eng. Sci.* **2002**, 57, 763.
- [78] N. Riphaut, P. Strobl, B. Stiaszny, T. Zinkevich, M. Yavuz, J. Schnell, S. Indris, H. A. Gasteiger, S. J. Sedlmaier, *J. Electrochem. Soc.* **2018**, 165, A3993.
- [79] S.-J. Choi, S.-H. Choi, A. D. Bui, Y.-J. Lee, S.-M. Lee, H.-C. Shin, Y.-C. Ha, *ACS Appl. Mater. Interfaces* **2018**, 10, 31404.
- [80] T. Liu, L. Zhang, J. Li, Y. Li, K. Lai, S. Zhang, G. Zhao, D. Liu, Z. Xi, C. Liu, L. Ci, *J. Electroanal. Chem.* **2023**, 928, 117032.
- [81] M. J. Kim, J. W. Park, B. G. Kim, Y. J. Lee, Y.-C. Ha, S. M. Lee, K. J. Baeg, *Sci. Rep.* **2020**, 10, 11923.
- [82] D. H. Kim, D. Y. Oh, K. H. Park, Y. E. Choi, Y. J. Nam, H. A. Lee, S.-M. Lee, Y. S. Jung, *Nano Lett.* **2017**, 17, 3013.
- [83] Y. Li, Y. Wu, Z. Wang, J. Xu, T. Ma, L. Chen, H. Li, F. Wu, *Mater. Today* **2022**, 55, 92.
- [84] N.-Y. Kim, J.-H. Kim, H. Koo, J. Oh, J.-H. Pang, K.-D. Kang, S.-S. Chae, J. Lim, K. W. Nam, S.-Y. Lee, *ACS Energy Lett.* **2024**, 9, 5688.
- [85] S. Wang, Y. Wu, T. Ma, L. Chen, H. Li, F. Wu, *ACS Nano* **2022**, 16, 16158.
- [86] Y. Wu, W. Zhang, X. Rui, D. Ren, C. Xu, X. Liu, X. Feng, Z. Ma, L. Lu, M. Ouyang, *Adv. Energy Mater.* **2025**, 15, 2405183.
- [87] M. Ahuis, S. Doose, D. Vogt, P. Michalowski, S. Zellmer, A. Kwade, *Nat. Energy* **2024**, 9, 373.
- [88] C. Li, H. P. Zhang, L. J. Fu, H. Liu, Y. P. Wu, E. Rahm, R. Holze, H. Q. Wu, *Electrochim. Acta.* **2006**, 51, 3872.

- [89] X. Lin, Y. Zhao, C. Wang, J. Luo, J. Fu, B. Xiao, Y. Gao, W. Li, S. Zhang, J. Xu, F. Yang, X. Hao, H. Duan, Y. Sun, J. Guo, Y. Huang, X. Sun, *Angew. Chem., Int. Ed.* **2024**, *63*, 202314181.
- [90] Y. Hu, J. Fu, J. Xu, J. Luo, F. Zhao, H. Su, Y. Liu, X. Lin, W. Li, J. T. Kim, X. Hao, X. Yao, Y. Sun, J. Ma, H. Ren, M. Yang, Y. Huang, X. Sun, *Matter* **2024**, *7*, 1018.
- [91] Z. Huang, S. Yoshida, H. Akamatsu, K. Hayashi, S. N. Ohno, *ACS Mater. Lett.* **2024**, *6*, 1732.
- [92] D. R. Sadoway, S. N. Flengas, *Can. J. Chem.* **1978**, *56*, 2013.
- [93] F. W. Poulsen, N. H. Andersen, K. N. Clausen, D. R. Sadoway, L. H. Øgødal, *Solid State Ionics* **1988**, *28–30*, 271.